Thermal Response of a Conceptual Deep Geological Repository in Sedimentary Rock

NWMO-TR-2018-09 April 2018

Ruiping Guo

Nuclear Waste Management Organization

nwmo
NUCLEAR WASTE MANAGEMENT ORGANIZATION
SOCIÉTÉ DE GESTION DES DÉCHETS NUCLÉAIRES

Nuclear Waste Management Organization
22 St. Clair Avenue East, 6th Floor
Toronto, Ontario
M4T 2S3
Canada

Tel: 416-934-9814
Web: www.nwmo.ca

Thermal Response of a Conceptual Deep Geological Repository in Sedimentary Rock

NWMO-TR-2018-09

April 2018

Ruiping Guo
Nuclear Waste Management Organization

Document History

Title:	Thermal Response of a Conceptual Deep Geological Repository in Sedimentary Rock		
Report Number:	NWMO-TR-2018-09		
Revision:	R000	Date:	April 2018
Nuclear Waste Management Organization			
Authored by:	Ruiping Guo		
Verified by:	Scott Briggs		
Reviewed by:	Neale Hunt, Tom Lam, Alan Murchison		
Approved by:	Paul Gierszewski		

ABSTRACT

Title: **Thermal Response of a Conceptual Deep Geological Repository in Sedimentary Rock**
Report No.: **NWMO-TR-2018-09**
Author(s): Ruiping Guo
Company: Nuclear Waste Management Organization
Date: April 2018

Abstract

The NWMO is designing and assessing the thermal-mechanical performance of a deep geological repository (DGR) in a sedimentary rock environment, in which used fuel containers are horizontally placed in buffer boxes perpendicular to the placement room axis. This report assesses the thermal performance of the conceptual DGR and its placement concept.

A series of design studies for conceptual deep geological repositories has been carried out over the past 30 years. These include two- and three-dimensional thermal transient and thermo-mechanical analyses for the far-field and near-field regions. In the near-field models, an adiabatic thermal boundary condition is applied on the four vertical outside model boundaries and as such, this represents a repository with an infinite horizontal dimension. The results from such models are accurate at early times with the thermal response overestimated at longer times.

In this report, Near-Field and Far-Field Models are created using the COMSOL code and used to perform thermal modelling. Results are then corrected to account for the influence of the adiabatic boundary condition.

The results show, for the conceptual design considered, that the maximum container surface temperature is 93°C after 47 years, the maximum temperature at the placement room centre is 92°C after 47 years and the maximum rock temperature (occurring at the roof above the container) is 85°C after 68 years.

TABLE OF CONTENTS

LIST OF TABLES

Page

LIST OF FIGURES

Page

1. INTRODUCTION

The Nuclear Waste Management Organization (NWMO) is responsible for the long-term management of Canada's used nuclear fuel. The adopted approach includes placement of the used fuel in a deep geological repository (DGR), hosted in either crystalline or sedimentary rock (NWMO 2005).

A DGR is a multiple-barrier system designed to safely contain and isolate used nuclear fuel over the long term. Based on the current reference design, it will be constructed at a depth of approximately 500 metres, depending upon the specific geology and detailed characteristics of the site. It consists of a network of placement rooms for the used-fuel containers and clay-based sealing systems, as well as a series of access tunnels and shafts to ensure accessibility and monitoring. The layout of the repository will depend on a number of factors, including the characteristics of the host rock, refinements made to the final design of the engineered-barrier system, final safety considerations, and the inventory of used fuel to be managed.

The used-fuel containers are encased within a bentonite buffer box which will be placed horizontally in the placement rooms. Spaces between individual buffer boxes will be filled with highly compacted bentonite spacer blocks while gaps between the buffer boxes/spacer blocks and the excavation wall will be filled with bentonite pellets. Concrete and clay-based bulkheads will be placed at strategic locations in tunnels and shafts and at the entrance to each placement room.

One of the important considerations for repository designers is the heat given off by radioactive decay of the used fuel.

The temperature increase caused by heat input from the used fuel can affect many aspects of near-field and far-field behaviour. For example, the induced heat load and associated temperature variation can change the mechanical behaviour of the rock (Ranjith et al. 2012), and thermal expansion of both the solid constituents and the water in the surrounding rock pores can create a potential for increased rock damage near the underground openings (Read et al. 1997). Rock pore water pressure changes induced by thermal expansion influence both the rock stresses and the hydraulic gradients. Increased pore water pressure in the rock will result in an increase in tensile stress with potential to cause tensile fracturing (Berchenko et al. 1997). Non-uniform pore water pressure increase can alter the existing hydraulic gradients and can affect both the quantity of flow through the rock and the flow direction, thus potentially affecting the advective transport of water-borne radionuclides (Dixon et al. 2002).

The temperature increase in the used-fuel containers, buffer materials and the surrounding rock also changes the moisture content of the clay-based sealing materials, thus resulting in changes in thermal parameters which, in turn, influence the overall thermal response of the repository (Dixon et al. 2002). The used-fuel container corrosion rate also depends on the thermal response in the repository (King 2013).

These factors are addressed in the DGR design. In particular, an important design basis is that the container spacing is selected in order to keep the container surface temperature below 100°C.

A series of conceptual design studies for a DGR has been carried out in the past (Acres et al. 1985, 1993; Mathers 1985; Tsui and Tsai 1985; Baumgartner et al. 1994; Park et al. 2000; Guo

2008; 2016; Hökmark et al. 2010). These studies include two- and three-dimensional thermal transient and thermo-mechanical analyses.

As it is not numerically practical to include near-field detail in a repository size model, the analyses are typically divided into near-field and far-field modelling. In the near-field models, an adiabatic thermal boundary condition is applied on the four vertical outside boundaries and as such, this represents a repository with an infinite horizontal dimension. For a finite dimension repository, results generated with this approach are accurate for early times with the thermal response overestimated at longer times (Guo 2007). To correct for this, Guo (2007, 2017) proposed a method for modifying near-field thermal results. This approach is applied in the present study to evaluate the thermal performance of a conceptual repository in sedimentary rock.

This report contains the following:

- Description of a proposed deep geological repository.
- Software, thermal equation, assumptions and material properties.
- The far-field model.
- The near-field model.
- Influences of other factors on the thermal results.
- Summary and conclusion

2. DESCRIPTION OF A PROPOSED DEEP GEOLOGICAL REPOSITORY

The site is hypothetical, but based on the general geological structure of the sedimentary rocks of the Michigan Basis of Southern Ontario. The assumed geological structure is described in Golder Associates Ltd. (2013). The conceptual DGR is proposed to be constructed at a depth of about 500 m below ground surface within the argillaceous limestone of the Cobourg Formation. This formation is known to have favorable properties, including good mechanical strength and very low permeability.

The conceptual DGR layout consists of an array of horizontal rectangular-shaped placement rooms (Figure 1). The placement room is 2.4 m high, 3.2 m wide and 341.6 m long (Gobien et al. 2017).

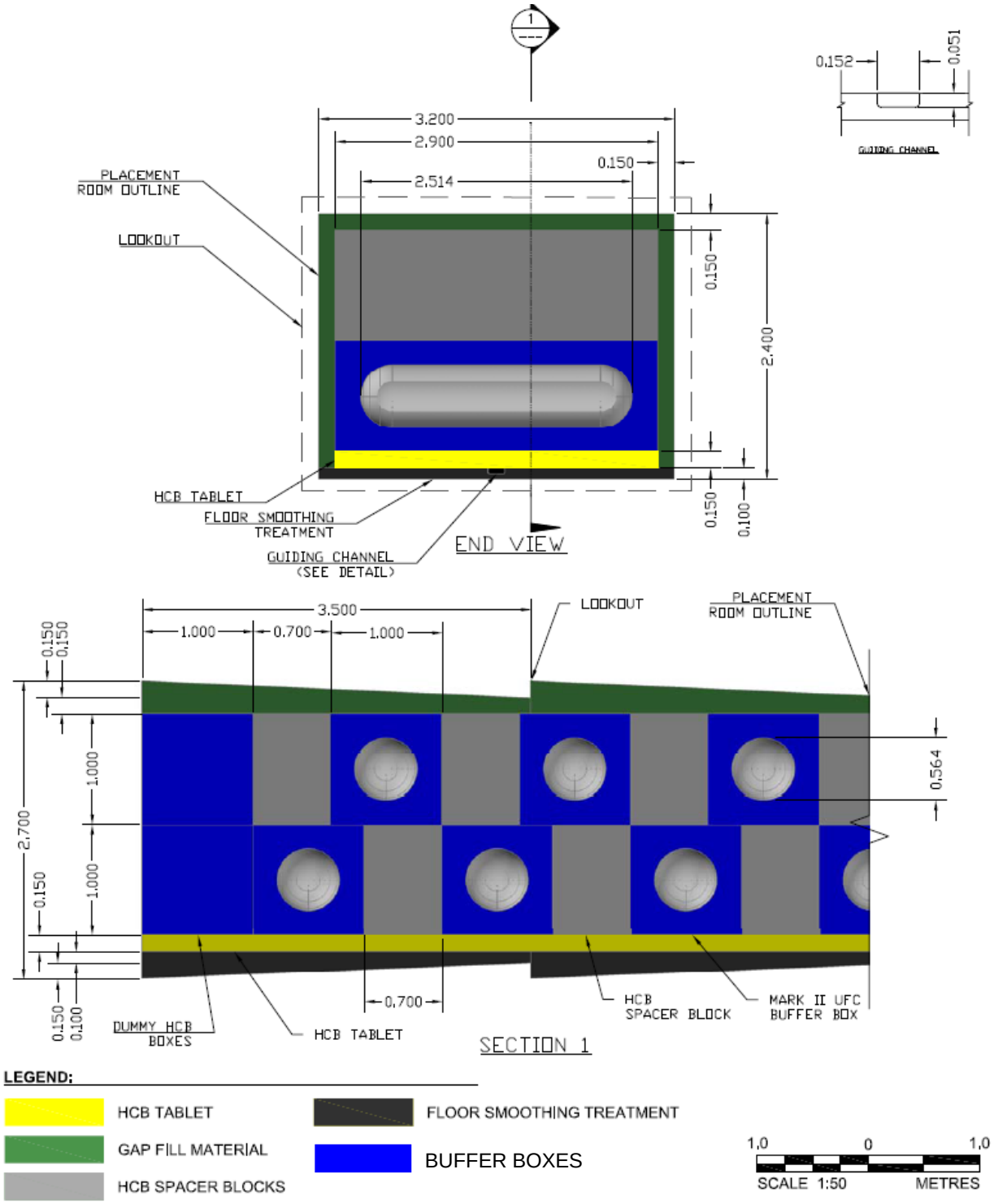

Source: APM-SPEC-01900-0204-R002

Figure 1: Sectional View of Placement Room

Access tunnels connect the placement rooms for moving personnel, material, excavated rock, used fuel storage containers and backfilling materials (Figure 2). In this conceptual model, the repository has 318 placement rooms arranged in ten panels, with two panels each having 16 placement rooms, two panels each having 35 placement rooms and six panels each having 36 placement room (Figure 2) The room spacing (centre to centre) is 25 m.

Each room contains a number (up to 376) of used-fuel containers placed in two layers. Each container is surrounded by highly compacted bentonite (to form a buffer box) and placed horizontally perpendicular to the tunnel axis (Figure 3). Between two bentonite boxes is a spacer block made of highly compacted bentonite.

Each container is 2.514 m long with a diameter of 0.564 m and can accommodate 48 used CANDU® fuel bundles. The container design consists of a 3-mm-thick copper outer corrosion-barrier and an inner, carbon-steel load-bearing component. The DGR has a minimum total capacity of about 5.224 million intact fuel bundles or about 108,834 used-fuel containers (UFCs). Dimensions of the repository, placement room, containers and sealing materials are shown in Figure 1 through Figure 3.

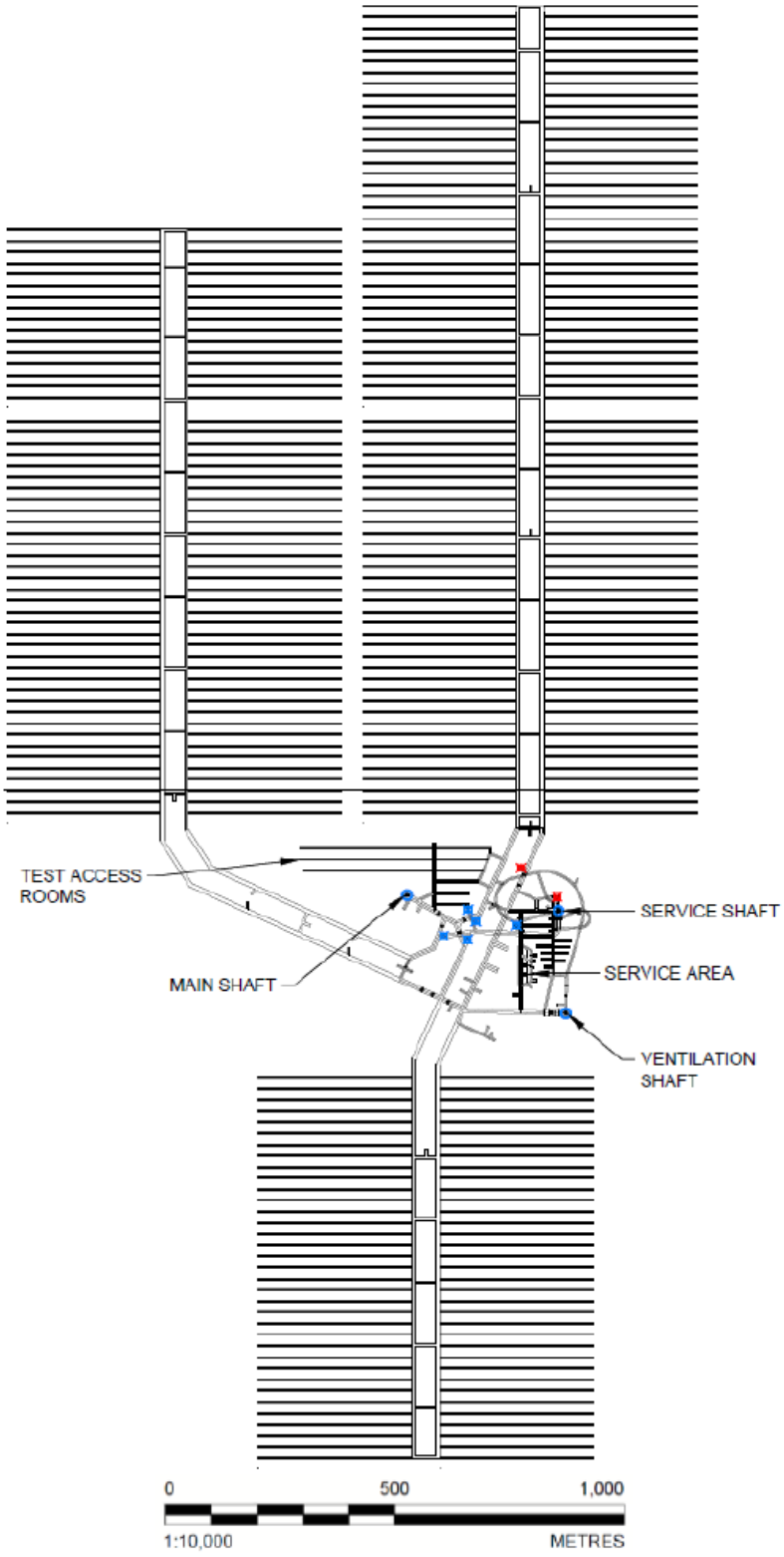

Source: APM-SPEC-01900-0204-R002

Figure 2: Sedimentary Underground Repository Layout for 5.224 Million Bundles

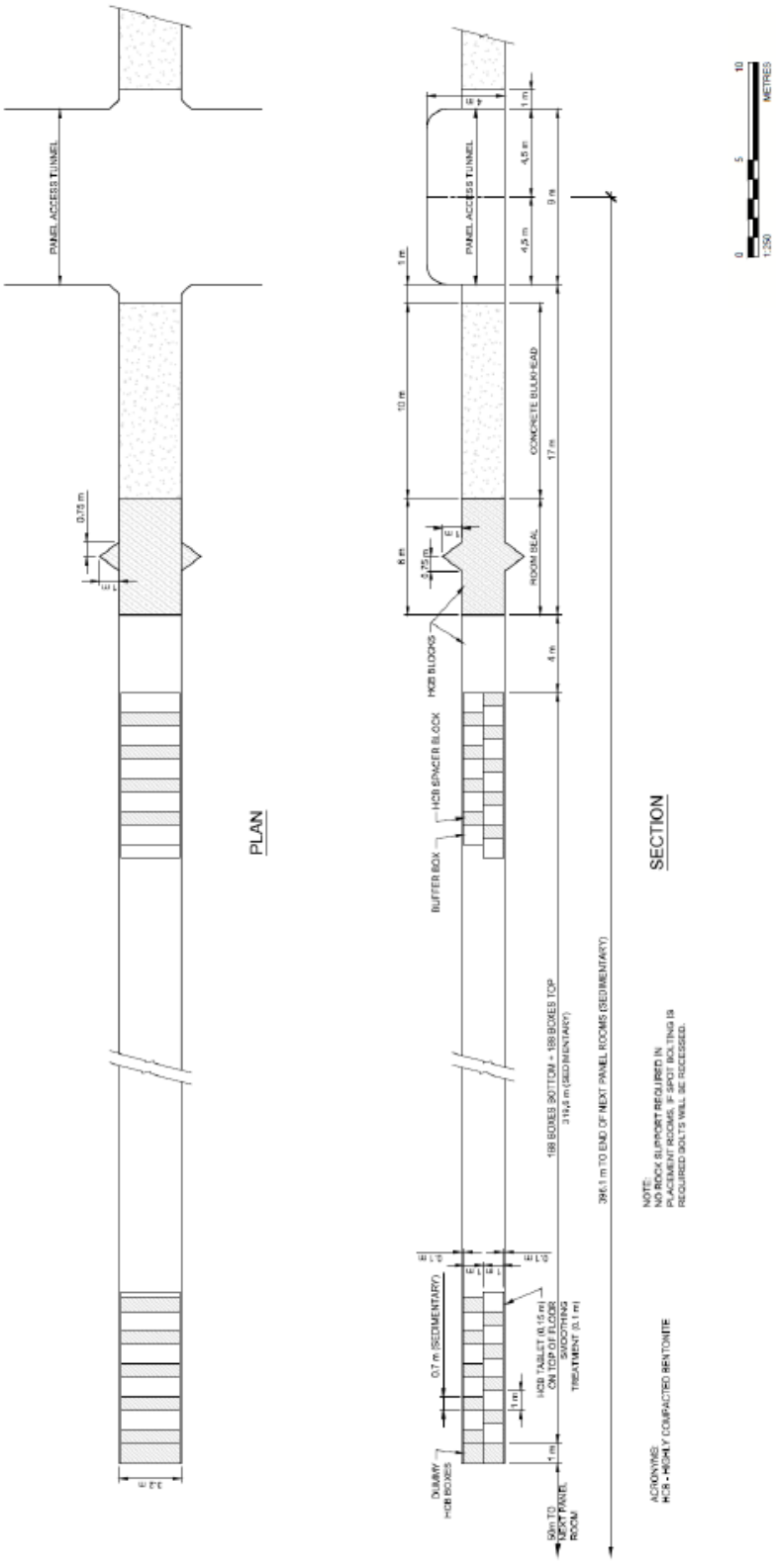

Source: APM-SPEC-01900-0204-R002

Figure 3: Plan View and Longitudinal Section of Placement Room

3. SOFTWARE, THERMAL EQUATION, ASSUMPTIONS AND MATERIAL PROPERTIES

3.1 SOFTWARE

COMSOL Multiphysics v5.3 is used to perform this modelling exercise. COMSOL Multiphysics is a finite element modelling environment used to model and solve all kinds of scientific and engineering problems (COMSOL 2017).

COMSOL is installed on a Dell Precision T7600 machine with Windows 7 professional running system with the following properties:

- Intel® Xeon® CPU E5-2680 @ 2.70 GHz (2 processors)
- 64GB (RAM)

3.2 THERMAL EQUATION

The following equation is used to solve the thermal transfer in the rock (COMSOL 2017).

$$\rho C_p \frac{\partial T}{\partial t} = \nabla \cdot (k \nabla T) + Q \qquad (1)$$

where ρ is the density (kg/m^3); C_p is the heat capacity (J/(kg·K)); k is the thermal conductivity (W/(m·K)); Q is the heat source or sink (W/m^3); T is the temperature (K); and t is the time after placement in the repository (s).

3.3 ASSUMPTIONS

The repository is assumed constructed at a depth of 500 m within the argillaceous limestone of the Cobourg Formation in a sedimentary sequence of carbonate and shale of approximate 680-m depth. Each of the rock materials is assumed homogeneous and isotropic with temperature-independent properties. The rock mass around the DGR is assumed infinite in the horizontal extent. The DGR is assumed to be filled instantaneously with 30-year-out-of-reactor fuel at the reference conditions.

3.4 MATERIAL PROPERTIES

USED-FUEL PROPERTIES

The heat output from the used fuel in each used fuel container is shown in Table 1 (Tait et al. 2000). All used fuel is assumed to have a burnup of 220 MWh/kgU and to undergo an initial cooling period of 30 years prior to placement.

Table 1: Heat Output of a Container of Reference Used CANDU Fuel (220 MWh/kgU Burn-up**) at Different Times**

Time out-of-reactor (years)	Q per container (W/container) (48 bundles)	Time out-of-reactor (years)	Q per container (W/container) (48 bundles)
30	169.1	200	38.72
35	155.2	300	32.80
40	142.3	500	26.89
45	131.2	1000	18.67
50	122.0	2000	12.75
55	112.7	5000	9.24
60	105.3	10000	6.64
70	91.57	20000	3.84
75	85.93	35000	2.10
80	80.85	50000	1.32
90	72.26	100000	0.407
100	65.33	200000	0.152
110	59.78	250000	0.140
135	49.99	500000	0.137
150	46.11	1000000	0.137
160	44.08		

ROCK-MASS PROPERTIES

The stratigraphy of the hypothetical site was created based on site characterization boreholes (DGR-1 to DGR-8) (Intera 2011) drilled at Bruce nuclear site for another project. The conceptual repository is assumed located in the low porosity limestone of the Cobourg Formation.

The thermal properties of selected geological units in the sedimentary rock are listed in Table 2 (Radakovic-Guzina et al. 2015). The density of the rock mass is 2,700 kg/m^3.

Table 2: Thermal Properties for the Units in the Sedimentary Rock

Geological unit	Unit top depth (m)	Thickness (m)	Thermal conductivity (W/(m·K))		Specific heat (MJ/(m^3·K))	
			Average	Model values	Average	Model values
drift	0	29.4		4.47		3.36
Unit B and C	29.4	52.3	2.22	2.42	2.5	2.50
Unit A-2 Carbonate	81.7	27	2.58		2.36	
Unit A-1 Upper Carbonate	108.7	3.0				
Unit A-1 Carbonate	111.7	22.1				
Unit A-1 Evaporate	133.8	2.0	5.31		4.11	
Unit A0	135.8	2.3				
Guelph	138.1	71.4		2.55		1.83
Reynales/Fossil Hill	209.5	6.8				
Cabot Head	216.3	15.8		1.89		1.79
Manitoulin	232.1	15.6		1.89		1.79
Queenstone	247.7	77.6	1.89	1.89	1.79	1.79
Georgian Bay / Blue Mountain	325.3	154.3	1.89	1.89	1.27	1.27
Cobourg	479.6	46.4	2.27	2.27	1.63	1.63
Sherman Fall	526	47.3	1.9	1.9	1.61	1.61
Kirkfield	573.3	39.5	2.28	2.28	2.07	2.07
Coboconk	612.8	8.0	6.11	2.78	1.99	1.99
Gull River	620.8	53.4	2.73		2.17	
Shadow Lake	674.2	7.6		3.00		2.28
Upper Precambrian	681.8	20		3.00		2.28
Precambrian	701.8			3.00		2.28

SEALING-MATERIAL AND USED-FUEL CONTAINER PROPERTIES

There are three bentonite clay-based sealing materials: buffer box material, highly compacted bentonite spacer blocks and buffer pellets. The buffer is placed around the container in the form of close-fitting, pre-compacted bentonite boxes. The material placed between two buffer-boxes is compacted bentonite slabs (bentonite spacer blocks). The buffer boxes and the spacer blocks (slabs) consist of highly compacted bentonite. The gap between the buffer boxes/spacer blocks and the tunnel surface is filled using a pelletized form of the buffer material. The specifications for the basic physical properties of clay-based sealing materials are presented in Table 3 (Baumgartner 2006). In this modelling exercise, the initial thermal parameters are used for the bentonite materials. Based on the study in Guo (2011), these values should produce conservative thermal results.

The thermal conductivity, density and specific heat of the used-fuel container and repository concrete are also shown in Table 3 (Incropera and DeWitt 2002).

Table 3: Thermal Parameters for the Clay-based Sealing Materials and Container

Property	Highly compacted bentonite	Gap fill (bentonite Pellets)	Concrete	Container
Thermal conductivity (W/(m·K))	1.00	0.37	1.67	45
Specific heat (J/(kg·K))	1240	870	900	434
Bulk Density (kg/m^3)	1955	1439	2425	7800

4 THE FAR-FIELD MODEL

This section describes the Far-Field Model for the conceptual repository described above and illustrated in Figure 3. The repository has 318 placement rooms arranged in ten panels, with two panels each having 16 placement rooms, two panels each having 35 placement rooms and six panels each having 36 placement room (Figure 2). There are 376 buffer box positions available in each placement room. Therefore, the plan area of the each panel is 900 m by 320.3 m for six panels, 400 m by 320.3 m for two panels and 875 m by 320.3 m for another two panels. The depth of the bottom of the placement room from the ground surface is 500 m as shown in Figure 2 and Figure 3.

4.1 MODEL GEOMETRY, BOUNDARY CONDITIONS, INITIAL CONDITIONS

The far-field thermal analysis provides an assessment of the thermal conditions in the rock mass surrounding a repository of finite dimension.

4.1.1 Far-Field Model Geometry

An isometric view of the Far-Field Model is shown in Figure 4. The model is bounded vertically by the ground surface on the upper side and by a plane 10,000 m below the ground surface at the bottom. The horizontal dimensions of the model in the X- and Y-directions are 5,000 m x 7,000 m. These dimensions are sufficient such that the thermal response of the rock at the boundaries remains unaffected by the presence of the DGR during the simulation time period (see Section 4.2). The DGR is represented by ten panels with a 2-m-thick plate of material generating heat. The horizontal dimensions of one DGR panel are shown in Figure 5. The locations of each panel in the Far-Field Model are also shown in Figure 5.

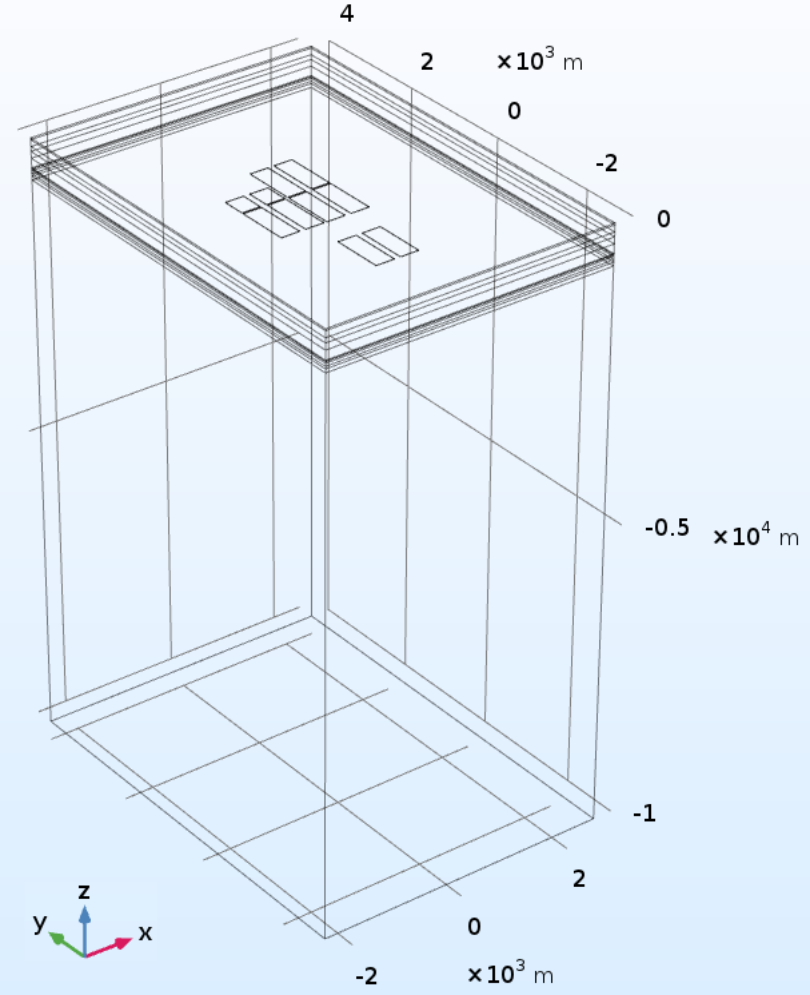

(Axis dimensions are in meters)

Figure 4: Isometric View of Far-Field Model

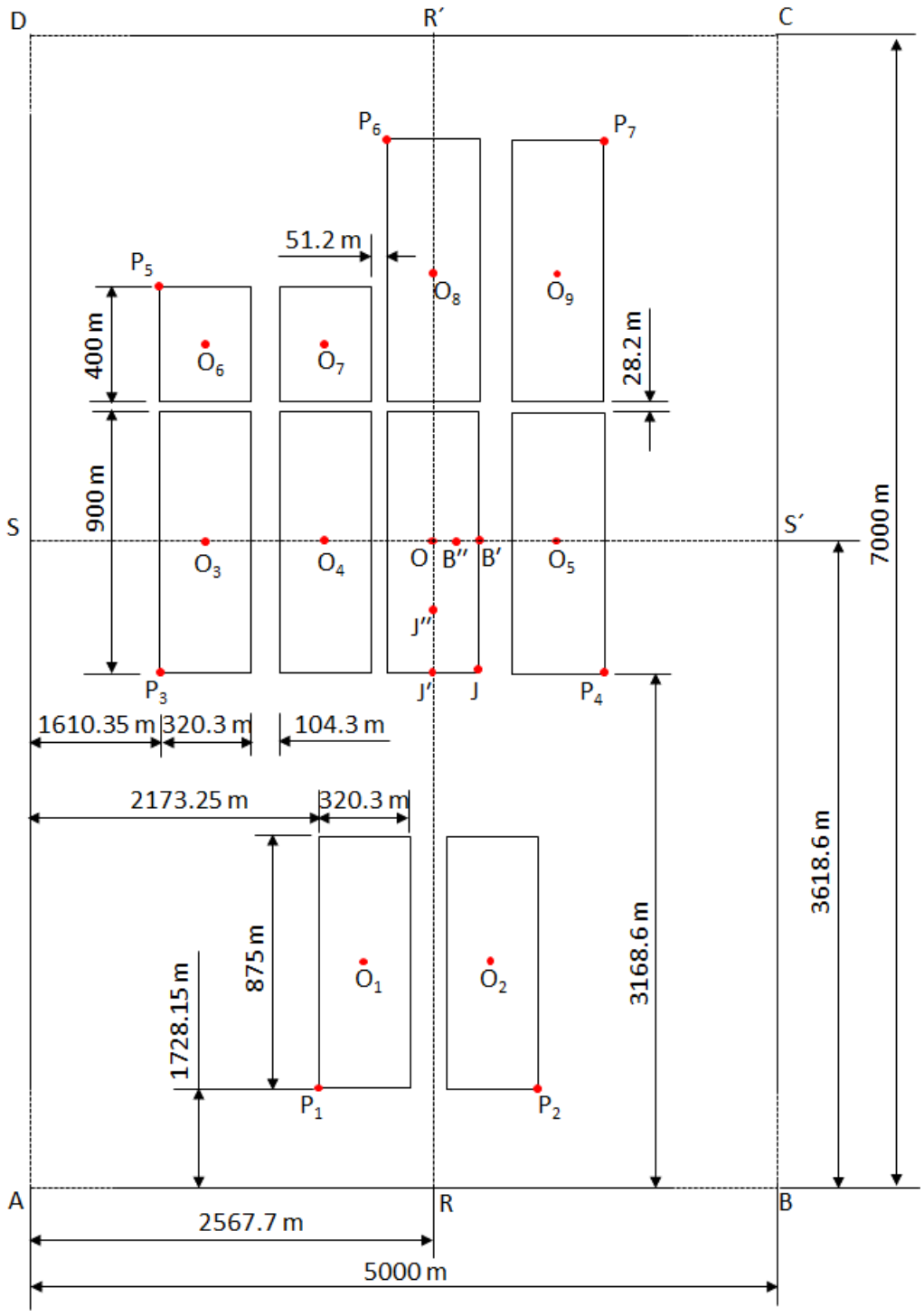

Figure 5: Cross Section of the Far-Field Model at Depth of 500 m from the Ground Surface

4.1.2 Far-Field Model Boundary Conditions

Thermal boundary conditions are defined as follows.

- The temperature on the ground surface is assumed to be 10°C (Intera 2011).
- The initial temperature of the rock at the repository horizon (500 m deep) is assumed to be 17°C (Intera 2011).
- The lower boundary is also modelled as an isothermal boundary set at a temperature of 113°C. The lower boundary temperature of 113°C is determined based on a steady study calculation without repository present using the thermal parameters defined in Table 2 and the surface temperature of 10°C and repository horizon initial temperature of 17°C.
- The vertical boundaries are modelled as adiabatic planes.
- The heat generated from the used-fuel containers is uniformly distributed throughout ten panel plates.

The model is representative of a finite size DGR positioned in an infinite extent of rock.

4.1.3 Initial Conditions for the Far-Field Modelling

The initial temperature is defined based on a steady calculation using the thermal parameters shown in Table 2 with the ground surface temperature of 10°C and the repository level initial temperature of 17°C. The initial temperatures for different depths are shown in Table 4. The initial temperature at other depths than listed in Table 4 is linear interpolated.

Table 4: Initial Temperature at Depth

Depth (m)	Temperature (°C)	Depth (m)	Temperature (°C)
0.0	10.0	479.6	16.7
29.4	10.2	526.0	17.3
138.1	11.6	573.3	18.0
185.0	12.1	612.8	18.6
216.3	12.5	674.2	19.2
325.3	14.2	10000.0	113.0

4.1.4 Finite Element Discretization

The finite-element discretization of the Far-Field Model is shown in Figure 6. The domain is discretized such that the elements are more densely distributed in the rock mass just above and beneath the repository level where the thermal gradients are expected to be the greatest. The model has 270,669 tetrahedral elements.

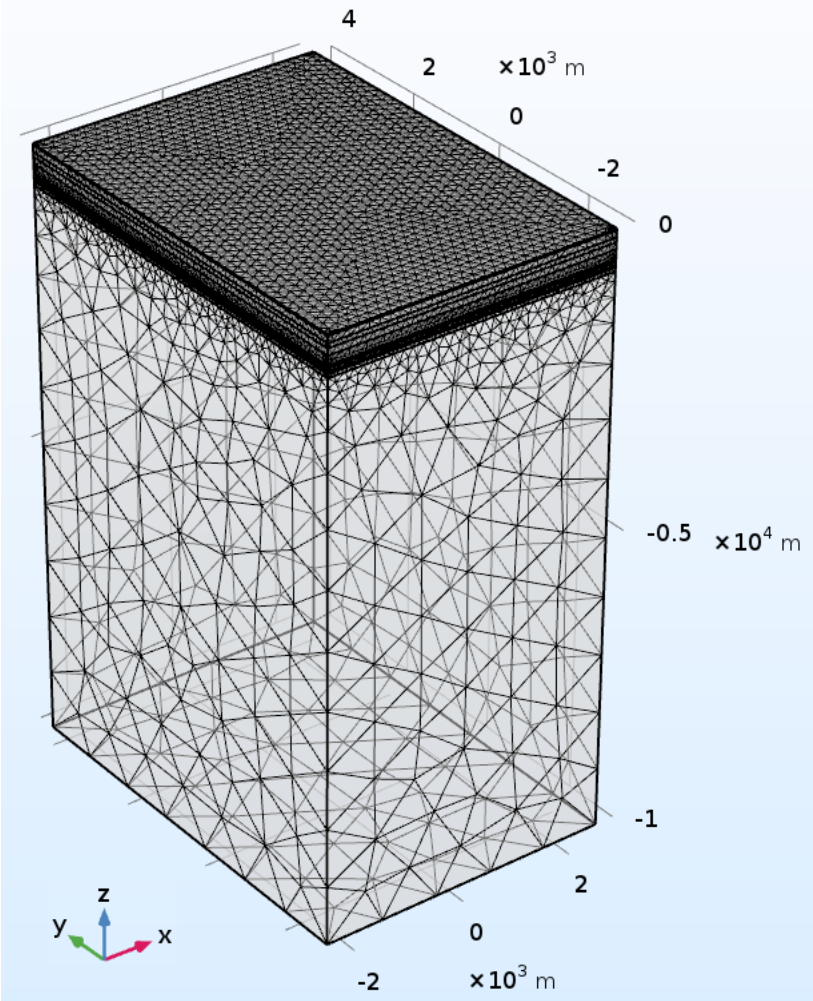

Figure 6: Mesh for the Far-Field Thermal Model

4.2 NUMERICAL RESULTS FROM FAR-FIELD MODELLING

Figure 7, Figure 8 and Figure 9 show the temperature along the horizontal cross section at a depth of 500 m from the ground surface after 87 years, 800 years and 10,000 years. The peak temperature at repository level is 79°C after 87 years, 75°C after 800 years, and 49°C after 10,000 years occurring at Point O (for location to see Figure 5).

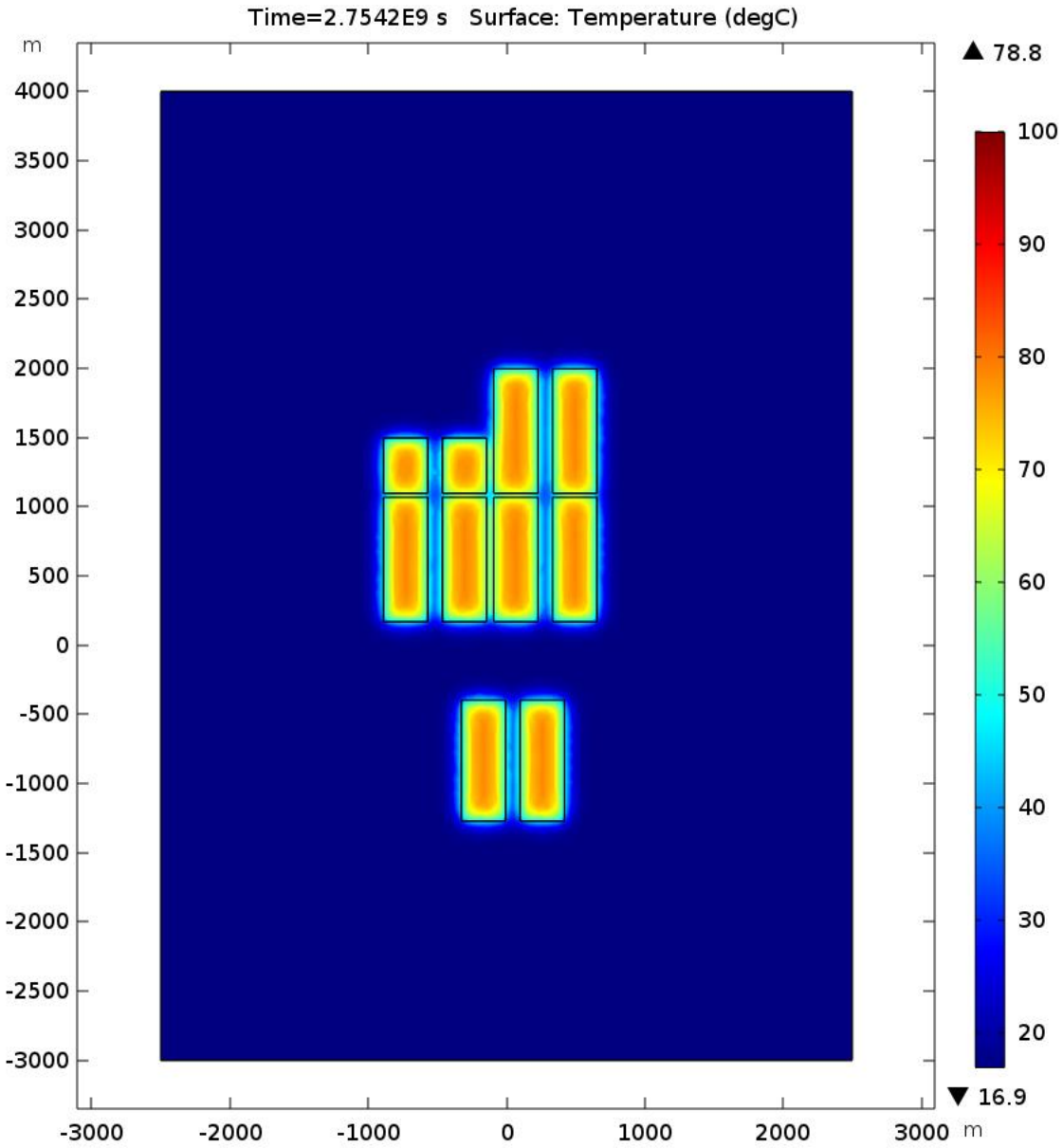

Figure 7: Temperature along Horizontal Cross Section at Depth of 500 m from Ground Surface at 87 Years after Placement

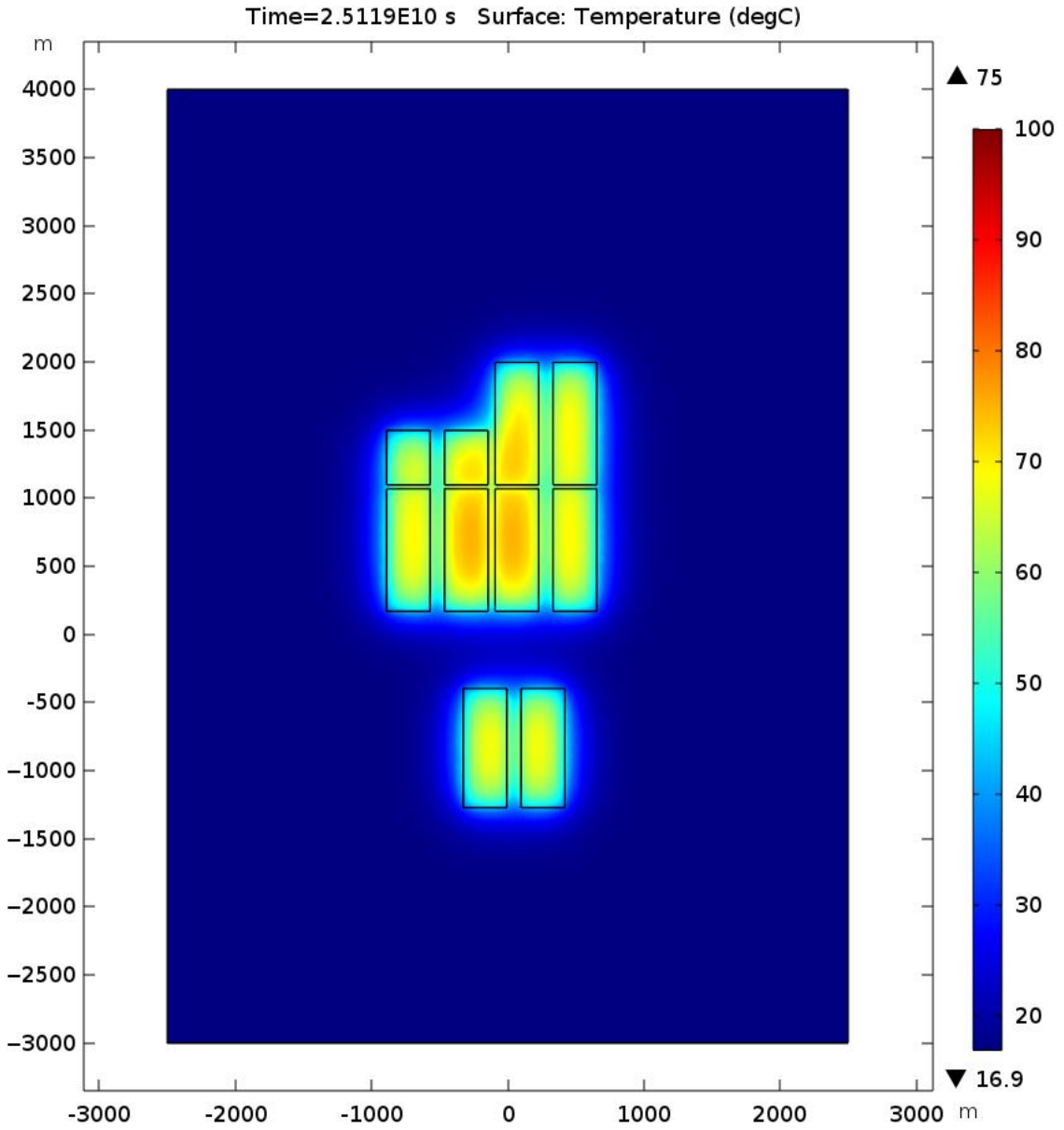

Figure 8: Temperature along Horizontal Cross Section at Depth of 500 m from Ground Surface at 800 Years after placement

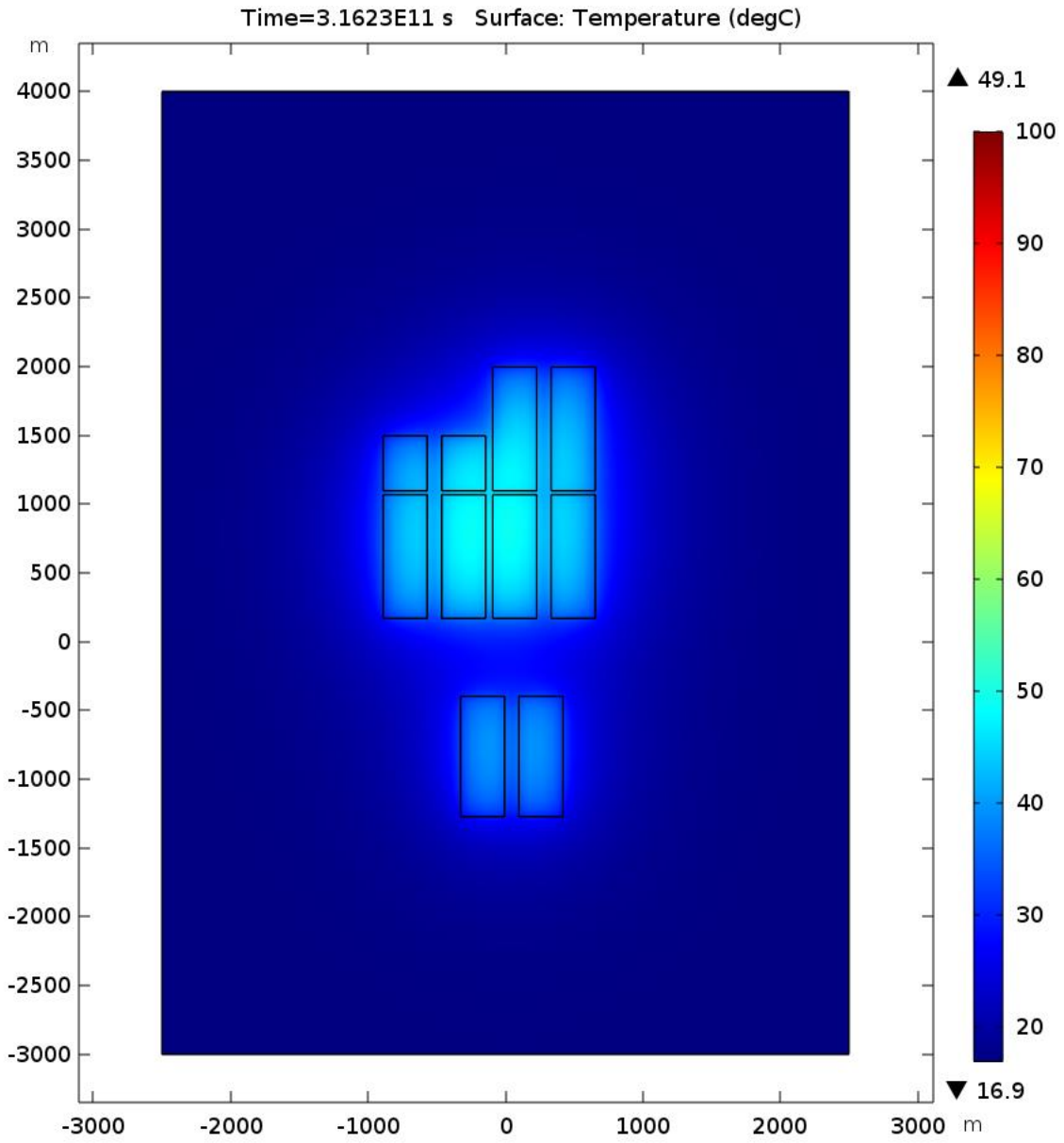

Figure 9: Temperature along Horizontal Cross Section at Depth of 500 m from Ground Surface at 10,000 Years after placement

Figure 10 illustrates the temperature at the six different locations O, B´, J, P_7, R and S (for locations see Figure 5). The first peak occurs at 87 years at the panel centre (Point O) with a magnitude of 79°C. The temperature at the panel centre is 75°C after 800 years, with the peak temperatures at the panel corners reaching 43°C (Point J) after 800 years and 36.5°C (Point P_7) after 69 years. The peak temperatures at Point R and Point S are 17.3°C at 40,000 years and 17.8°C at 30,000 years (their initial temperature is 17°C), which means that the model is of sufficient size to perform the thermal modelling.

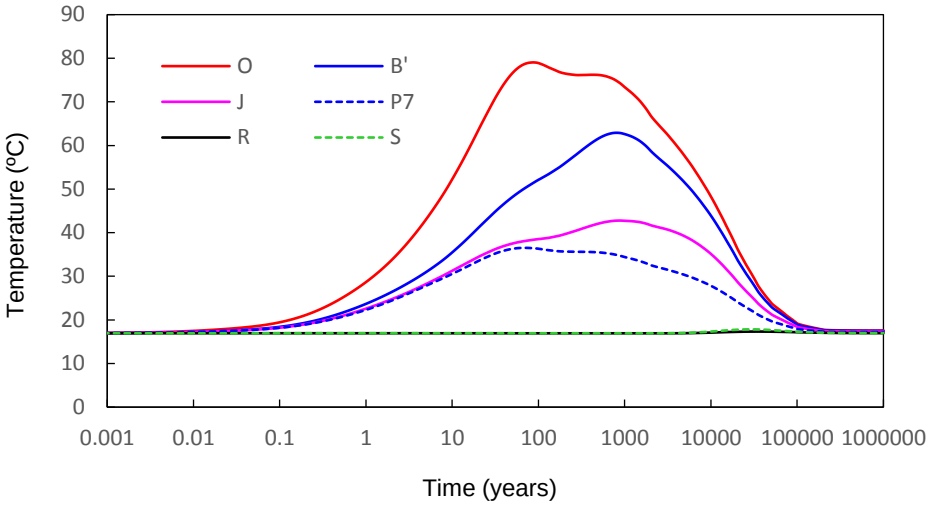

Figure 10: Temperature as a Function of Time at Different Points at Repository Level from Far-field Model

Figure 11 shows the temperatures as a function of time at different depths along the axis of the repository. The peak temperature at a depth of 5,000 m is 63°C at 100,000 years. Considering the initial temperature is 62.7°C, the influence of the repository is only 0.26°C, which means the vertical dimension of the model (10 km) is of sufficient size for the thermal modelling.

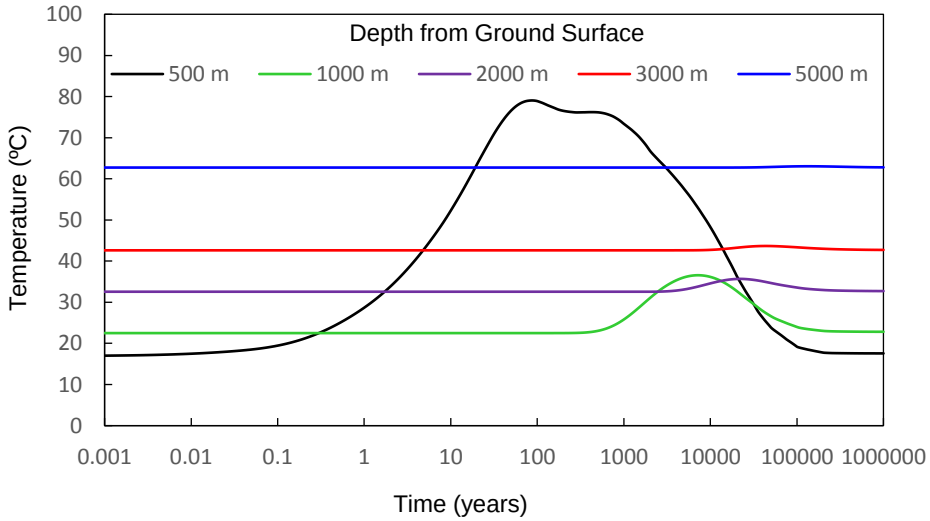

Figure 11: Temperature as a Function of Time at Different Points along the Vertical Line through Point O

Temperature profiles along the horizontal lines RR´ and SS´ (refer to Figure 5 for locations) at five different times are shown in Figure 12 and Figure 13. The thermal load influences the temperature of the rock in a range of 2,000 m or less from the centre of the boundary panel. Therefore, the horizontal dimension of 5,000 m by 7,000 m in the model is sufficient for the Far-Field Model.

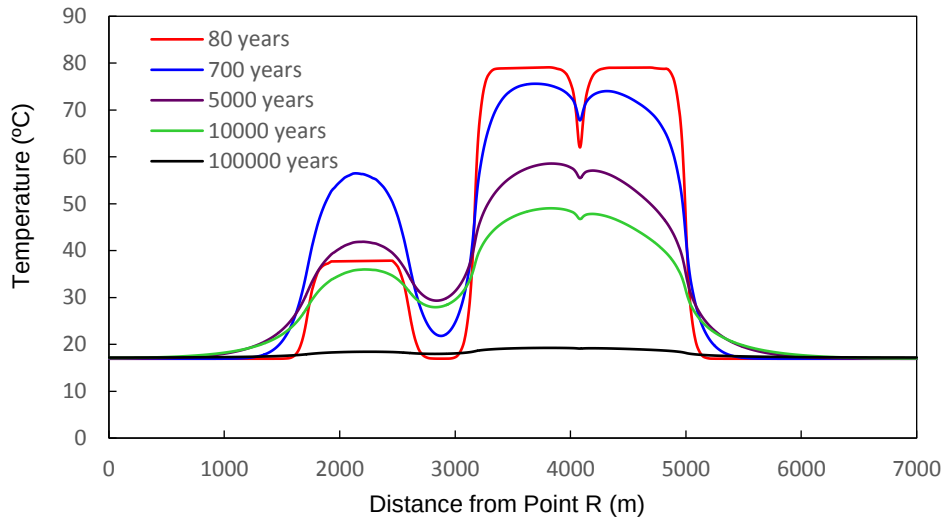

Figure 12: **Far-Field Temperature Profiles at Different Times along Horizontal Line RR′**

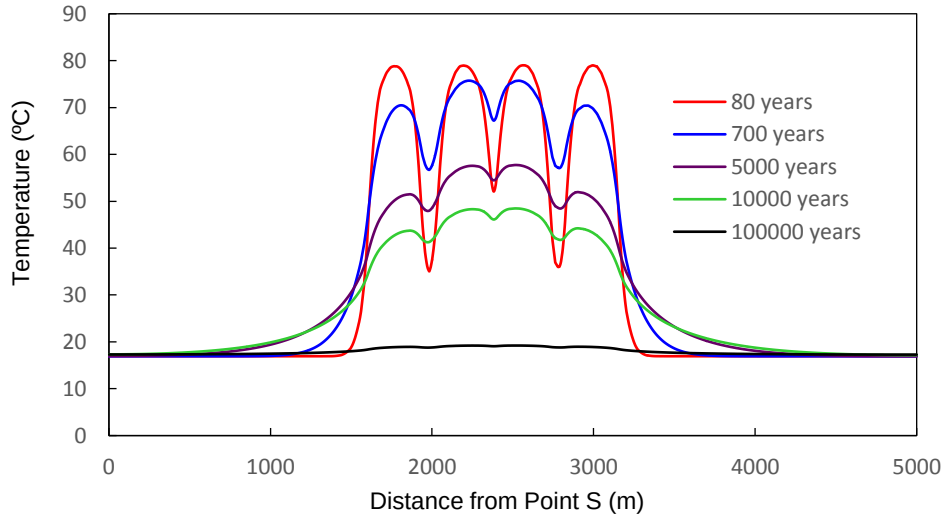

Figure 13: **Far-Field Temperature Profiles at Different Times along Horizontal Line SS′**

Figure 14 shows the far-field temperature profiles along vertical line through Point O. The depth at which the temperature is affected by the repository thermal load is about 3,000 m at 5,000 years after placement, 3,700 m at 10,000 years, and 8,000 m at 100,000 years.

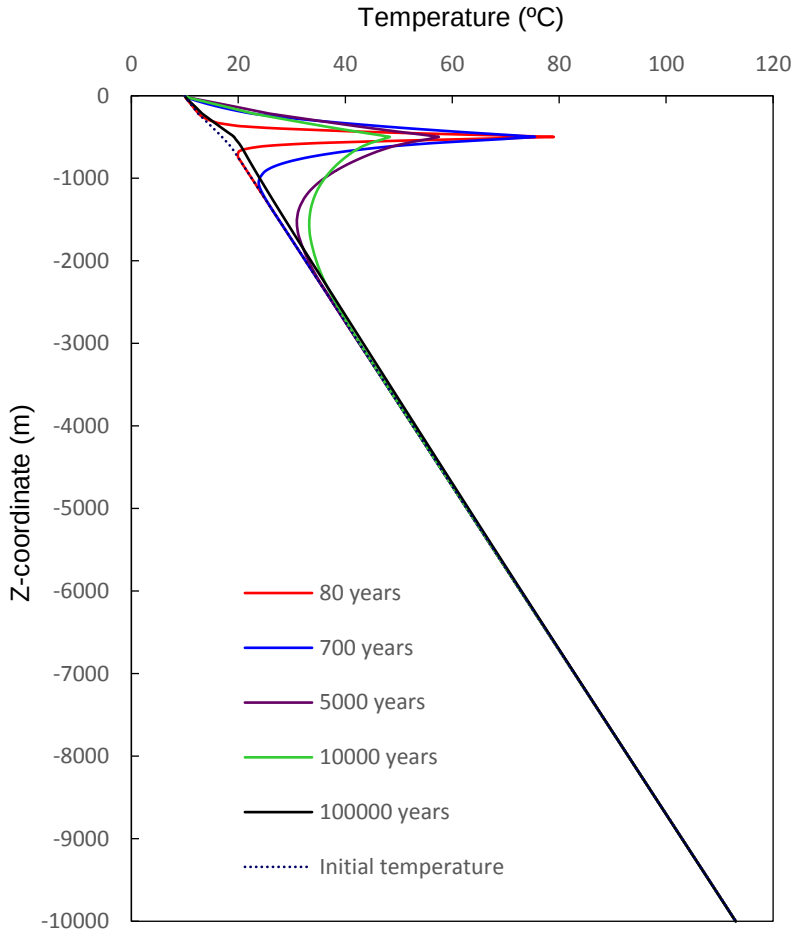

Figure 14: **Far-Field Temperature Profiles at Different Times along Vertical Symmetry Line through the Repository Centre**

In summary, the highest temperature in the repository is 79°C occurring at the panel centre (Point O) after 87 years, with a second peak of 75°C occurring after 800 years. The dimensions used in the Far-Field Model are large enough to carry out the far-field thermal modelling.

5 THE NEAR-FIELD MODEL

5.1 MODEL GEOMETRY AND BOUNDARY AND INITIAL CONDITIONS

5.1.1 Near-Field Model Geometry

The geometry of a unit cell for the Near-Field Model is shown in Figure 15. There are five kinds of materials: rock (10 layers of rock), bentonite buffer boxes and bentonite spacer blocks, concrete, container and bentonite pellets. The dimensions of the placement room are the same

as shown in Figure 1. The horizontal dimensions of a unit cell are 12.5 m x 1.7 m (1.7 m is the axial container spacing, 12.5 m is 1/2 of placement-room spacing). The vertical dimension of the model unit cell is 10,000 m. The depth of the bottom of the placement room is 500 m.

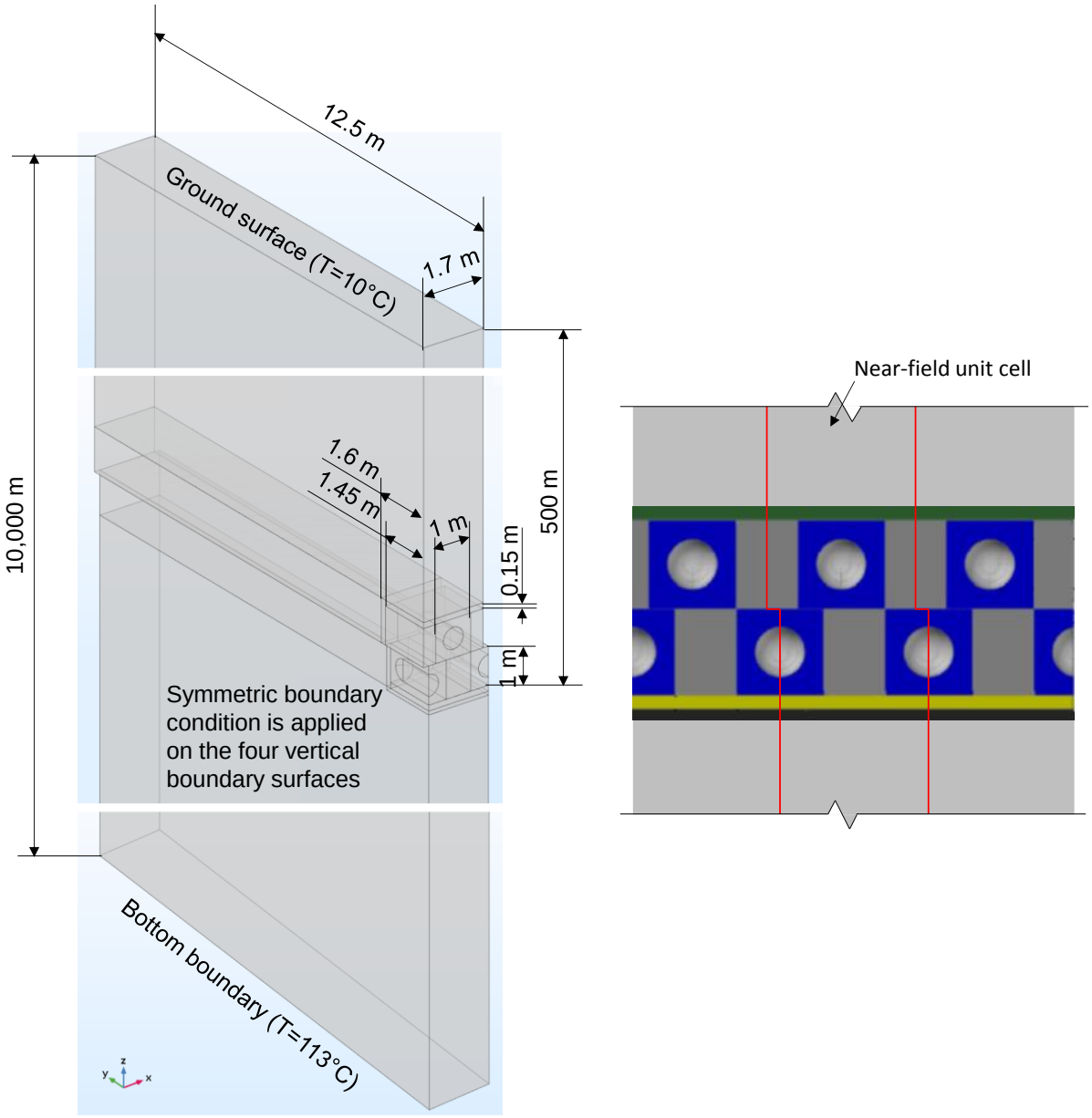

Figure 15: Geometry for Near-Field Unit Cell

Tetrahedral elements are used through the model. The elements are more densely distributed in the region of high thermal gradients as shown in Figure 16 (near the placement room), and with more detail in Figure 16. There are total 70,271 tetrahedral elements. Note that the upper section of the unit cell is horizontally offset by 0.15 m from the lower portion to make the outside surfaces be approximately symmetric.

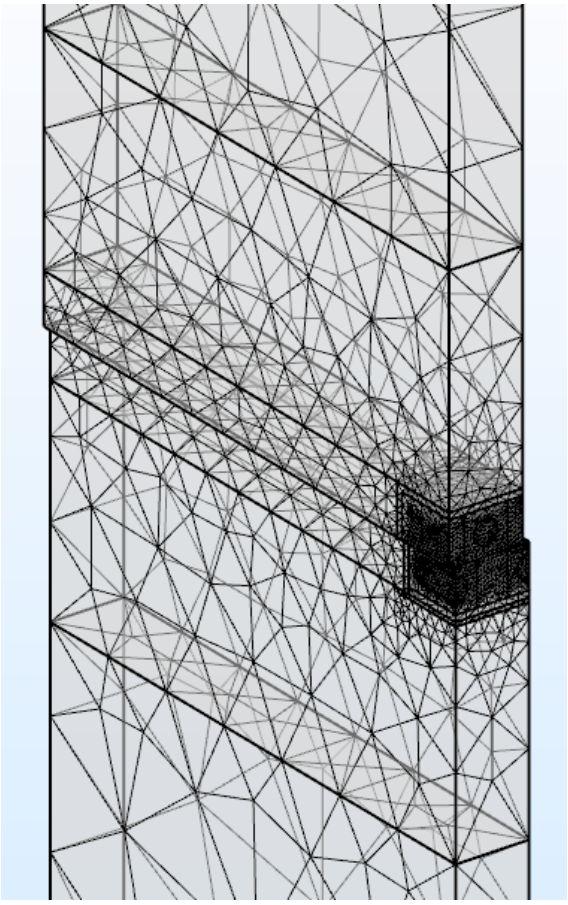

Figure 16: Finite Element Discretization of the Central Part of the Unit Cell for Near-Field Analyses

Figure 17 shows the locations at which the Near-Field Model results will be output in this report.

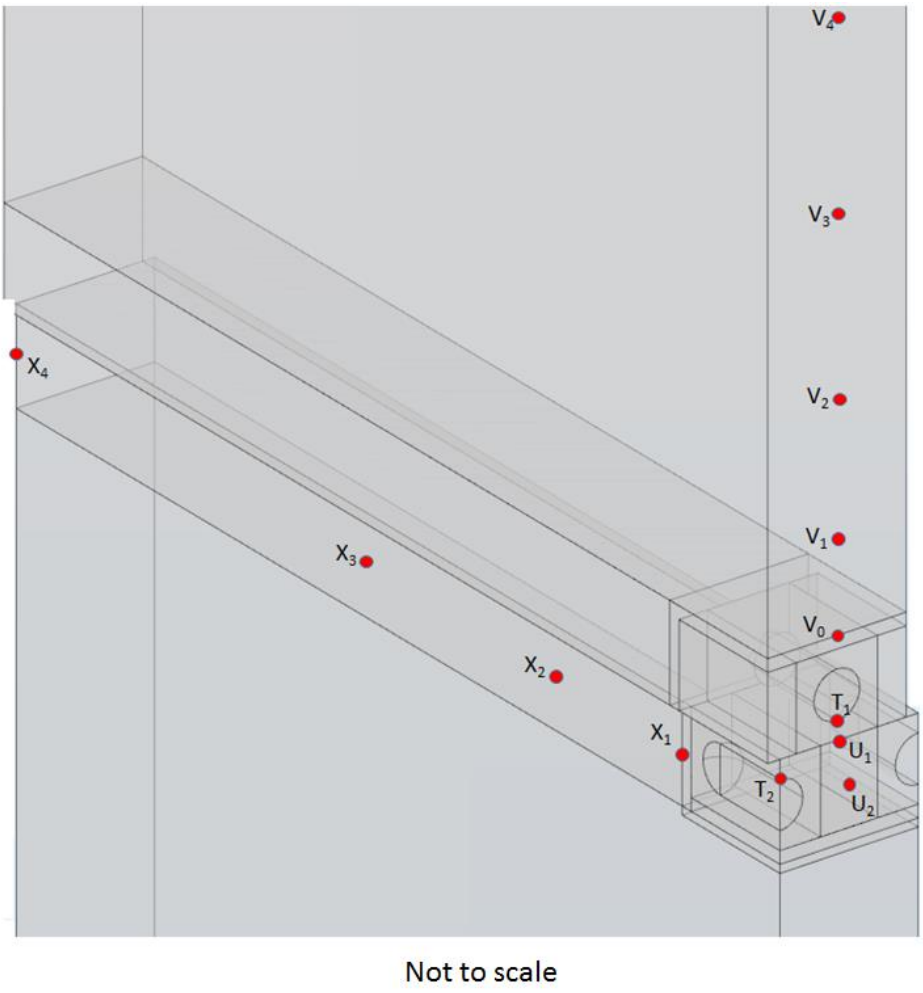

Figure 17: Locations at which the Near-Field Results Will Be Output in this Report

5.1.2 Boundary and Initial Conditions

5.1.2.1 Thermal Boundary Conditions

- The temperature on the ground surface is 10°C.
- The lower boundary is modelled as an isothermal boundary set at a temperature of 113°C. The lower boundary temperature of 113°C is determined based on a steady-state calculation using the thermal parameters defined in Table 2 with the surface temperature of 10°C and the repository initial temperature of 17°C.
- An adiabatic condition is applied on the four vertical surfaces of the model due to mirror symmetry although they are not entirely fully symmetric. This assumption will not influence

the container temperatures but it will have very minor influence on the buffer temperature (the influence is much less than 0.5°C based on a previous study[1]).

- A uniform thermal load is applied at the volume of two one-fourths of a container and one half of a container. The total thermal load applied is a container thermal load (Table 1).

The thermal boundary conditions described above represent boundary conditions for a unit cell in a horizontally infinite repository.

5.1.2.2 Initial Conditions

The initial temperature is defined based on a steady-state study using the thermal parameters show in Table 2 and the ground surface temperature of 10°C and the repository level initial temperature of 17°C. The resulting initial temperature is shown in Table 4. The initial temperature for depths other than those listed in Table 4 are determined via linear interpolation.

5.2 INFLUENCE OF THE ADIABATIC BOUNDARY CONDITION IN THE NEAR-FIELD MODEL

Based on the study in Guo (2016, 2017), the results from the Near-Field Model using such boundary conditions are accurate for early times, and overestimated at long times. Guo (2016, 2017) has proposed a method to correct for the effect of the adiabatic boundary condition.

The purpose of the Near-Field Thermal Modelling is to obtain the temperature $T_0 + \Phi_1$, where

- T_0 is the initial temperature which is consistent with the boundary conditions of the ground surface temperature and the model bottom temperature shown in Section 4.1.2; and
- Φ_1 is the temperature rise at any locations in a unit cell which is located at the centre of a repository panel and caused by the heat load released from the repository (Q_1) shown in Figure 18 (a). The temperature rise (Φ_1) meets the following equations (Holman 1976):

$$\frac{\partial \Phi_1}{\partial t} - \alpha \nabla^2 \Phi_1 = S_1 \quad (2)$$

$$\Phi_1(x, y, z, 0) = 0 \quad (3)$$

$$\Phi_1(x, y, 0, t) = 0 \quad (4)$$

where α is the thermal diffusivity of the medium, $\alpha = k/(\rho \cdot C_p)$, (m^2/s). S_1 is the heat source term ($Q/(\rho \cdot C_p)$) caused by repository heat load Q_1, (K/s).

[1] Personal communication with D. Marinceu, NWMO.

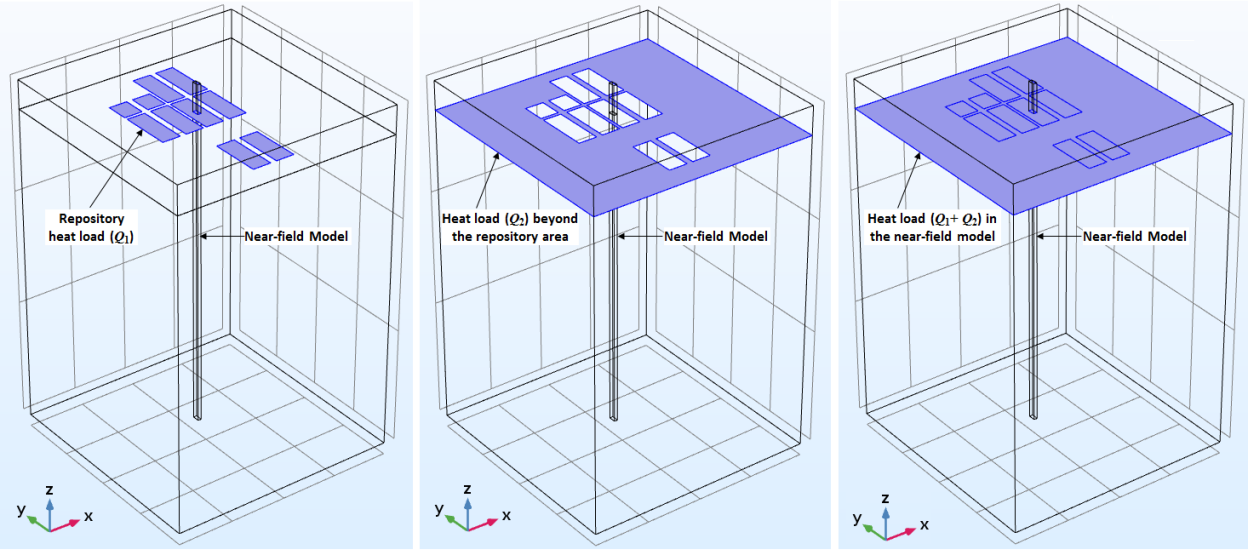

(a) Repository heat load (Q_1)

(b) Heat load (Q_2) caused by adiabatic boundary condition in the near-field model

(c) Heat load (Q_1+ Q_2) in the near-field model – infinite repository

Not to scale

Figure 18: Heat Load Terms related to the Near-Field Modelling

Due to the application of the adiabatic boundary condition on the outside surface of the Near-Field Model unit cell, the temperature in this unit cell effectively assumes that there are an infinite number of repeating adjacent heated cells. Therefore the calculated temperature rise in the unit cell not only includes the temperature rise (Φ_1) induced by the heat load from the repository (Q_1), but also includes an additional rise (ΔT) which is caused by heat load from the area beyond the repository (Q_2) due to the assumed repeating unit cell (Figure 18 (b)). This additional heat load Q_2 is an artefact of the unit cell model. The temperature rise ($\Phi_1+\Delta T$) from the near-field modelling meets the following equation:

$$\frac{\partial(\Phi_1+\Delta T)}{\partial t} - \alpha\nabla^2(\Phi_1+\Delta T) = S_1 + S_2 \quad (5)$$

$$(\Phi_1+\Delta T)(x,y,z,0) = 0 \quad (6)$$

$$(\Phi_1+\Delta T)(x,y,0,t) = 0 \quad (7)$$

where S_2 is the heat source term ($Q/(\rho \cdot C_p)$) caused by heat load Q_2, (K/s).

Subtracting (2) from (5), (3) from (6), and (4) from (7) gives:

$$\left(\frac{\partial(\Phi_1+\Delta T)}{\partial t} - \alpha\nabla^2(\Phi_1+\Delta T)\right) - \left(\frac{\partial\Phi_1}{\partial t} - \alpha\nabla^2\Phi_1\right) = (S_1+S_2) - S_1 \quad (8)$$

$$(\Phi_1+\Delta T)(x,y,z,0) - \Phi_1(x,y,z,0) = 0 \quad (9)$$

$$(\Phi_1+\Delta T)(x,y,0,t) - \Phi_1(x,y,0,t) = 0 \quad (10)$$

These become:

$$\frac{\partial(\Delta T)}{\partial t} - \alpha\nabla^2(\Delta T) = S_2 \quad (11)$$

$$\Delta T(x, y, z, 0) = 0 \quad (12)$$

$$\Delta T(x, y, 0, t) = 0 \quad (13)$$

Calculating ΔT for the geometry shown in Figure 18 (b) is not numerically practical if all repository details are incorporated. However, ΔT can be approximated by solving the geometry without considering the repository details. Specifically, ΔT also can be calculated using the following equation:

$$\Delta T = (\Phi_1 + \Delta T) - \Phi_1 \quad (14)$$

where $\Phi_1 + \Delta T$ is calculated for the geometry shown in Figure 18 (c) without considering the repository details based on Equations (5) – (7), which represents a repository with an infinite horizontal dimension. This can be solved using one–dimensional model or a small scale three dimensional model. Φ_1 is calculated from the Far-Field Model (Figure 18 (a)).

In this report a three-dimensional Simplified Near-Field Model is built to solve the one-dimensional problem. Using a three-dimensional model instead of using a one-dimensional model makes it easier to visualize the relationships between the Simplified Near-Field Model and the Near-Field Model and between the Simplified Near-Field Model and the Far-Field Model.

In the Simplified Near-Field Model (Figure 19 (a)), the geometry, initial conditions and boundary conditions are the same as those of the Near-Field Model. In this Simplified Near-Field Model, there is only one kind of material (rock), as in the Far-Field Model. The heat load is applied in the volume of the plate of 12.5 m x 0.75 m x 2 m located at a depth of 500 m. This approach ensures that the method of applying the heat load is the same as that in the Far-Field Model. Tetrahedral elements are used through the model. The elements are more densely distributed in the region near the placement room as shown in Figure 19 (b). There are a total of 85,920 tetrahedral elements.

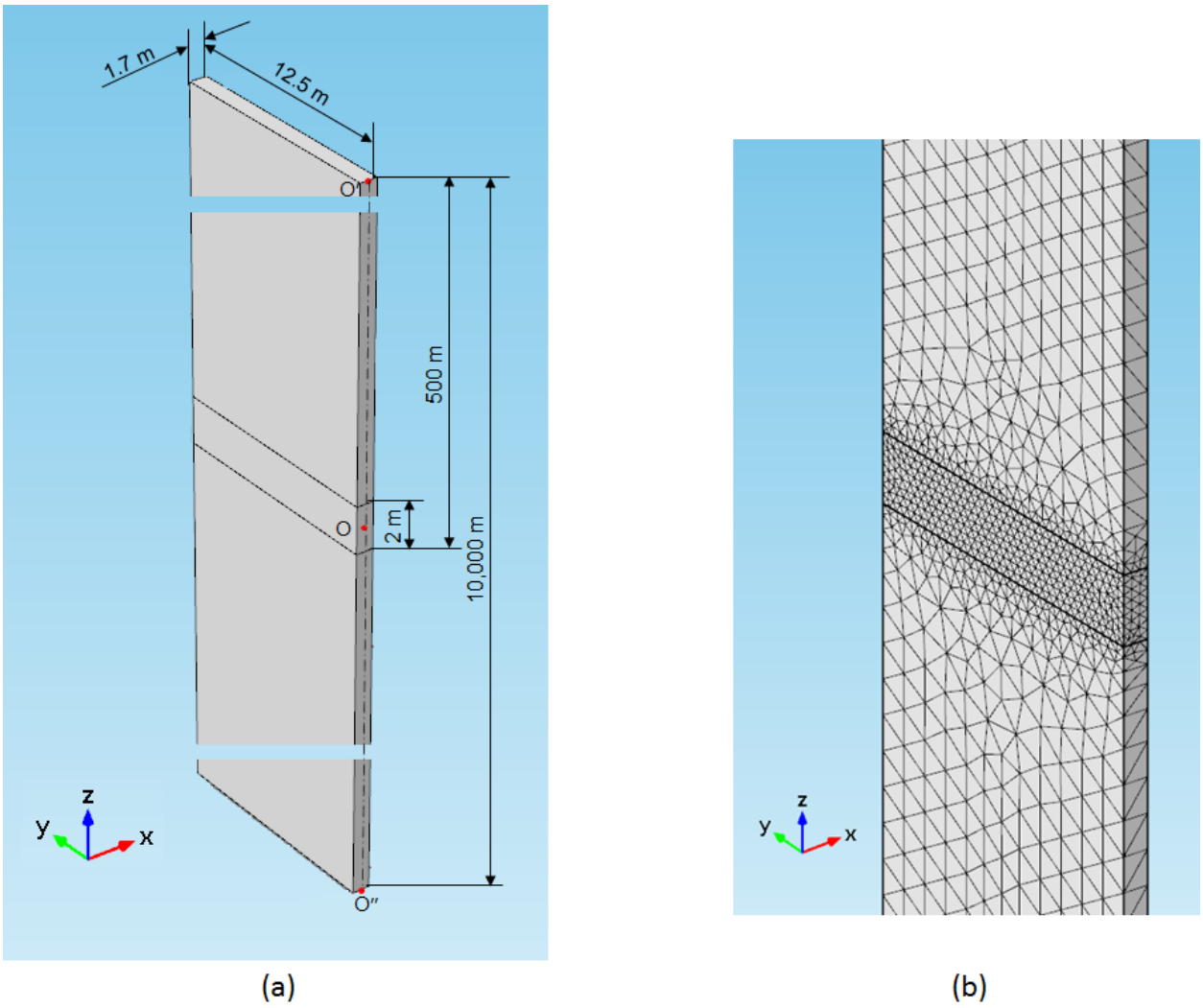

Figure 19: Geometry of the Simplified Near-Field Model and Mesh near the Repository Level

If a repository hosts many used fuel containers, a near-field unit cell (e.g., 12.5 m x 1.7 m) is small enough to be considered as a point compared to the area beyond the repository area in the infinite repository as described in the Simplified Near-Field Model. Therefore, the temperature increase caused by the heat load from the area beyond the finite repository (i.e., the adiabatic boundary condition influence) can be considered the same at any point of the Near-Field Model at the same depth (Guo 2017). Thus, the temperature difference along the vertical line through the panel centre (O) between the Simplified Near-Field Model and the Far-Field Model represents the influence of the thermal boundary conditions applied to the four vertical surfaces in the Near-Field Model (assuming that the Near-Field Model represents the unit cell located through the panel centre O).

Figure 20 shows the temperature difference at panel centre, O, between the Far-Field Model and the Simplified Near-Field Model. The Far-Field Model results represent the temperature changes induced by the heat load from the ten panels in the repository, while the temperature

for the Simplified Near-Field Model is caused by heat load not only from the ten panels but also from locations beyond the ten panel area (recall that the Simplified Near-Field Model is representative of an infinite repository). The difference in temperature is therefore representative of the boundary condition effect on the Near-Field Model, and this difference can be subtracted from the Near-Field Model results to remove the effect of the boundary condition. The maximum difference reaches 20°C after 10,020 years.

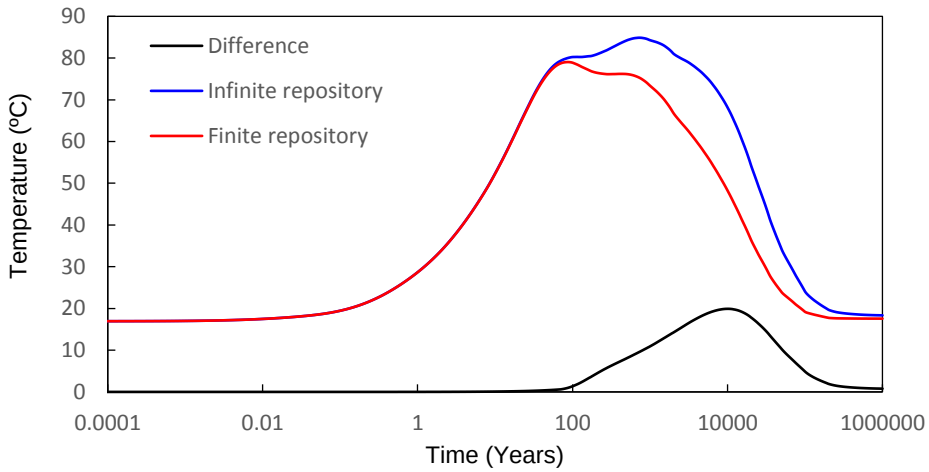

Figure 20: Temperature at Panel Centre (O) from the Far-field Model and Temperature at Repository Depth from the Simplified Near-Field Model and their Differences

Figure 21 shows temperature difference profiles along a vertical line through panel centre O between the Far-Field Model and the Simplified Near-Field Model. The temperature difference changes not only with time but also with depth. It can be expressed as:

$$\Delta T = \Delta T(t, z) \tag{15}$$

in which ΔT is the temperature difference between the Far-Field Model and the Simplified Near-Field Model, °C; t is time, second; z is the depth from the ground surface, m.

The Near-Field Model results can be obtained by subtracting the temperature difference (Equation (16)) from the infinite near-field results to erase the influence of the adiabatic boundary conditions.

$$T_n = T_{in} - \Delta T \tag{16}$$

in which T_n is the near-field temperature, °C; T_{in} is the results from the infinite near-field modelling.

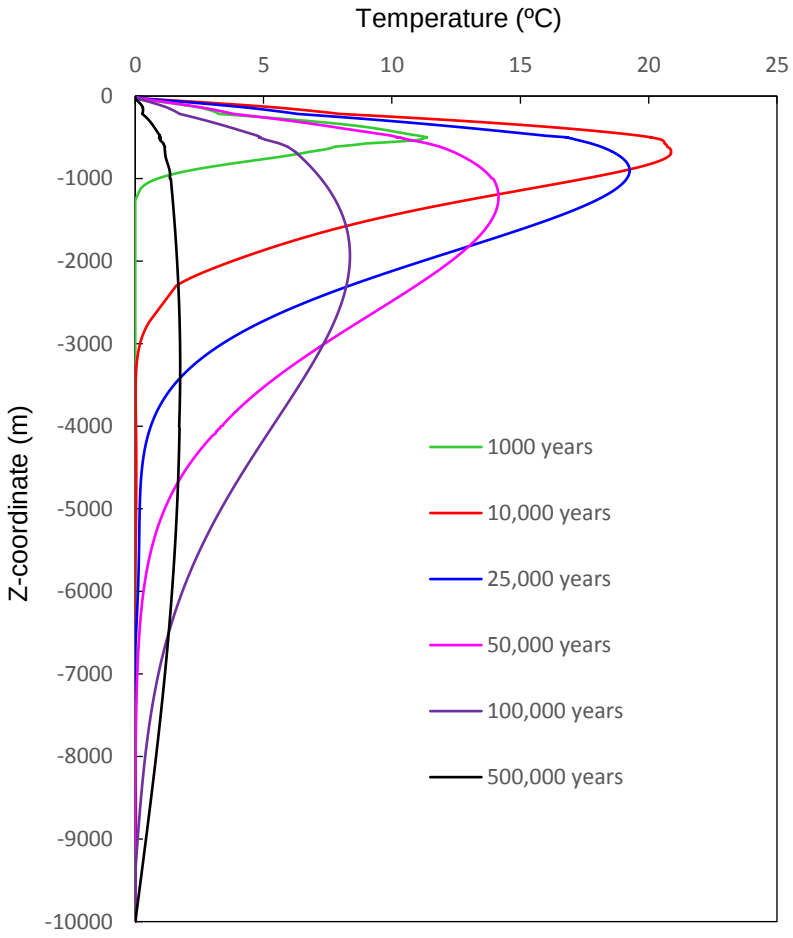

Figure 21: Temperature Difference Profiles along Vertical Line through Panel Centre O between the Far-field Model and the Simplified Near-Field Model

Theoretically, the method can be applied to obtain the temperature for a unit cell at any location in the repository panels. However, the modified analysis is useful to apply to a unit cell at the panel centre as this is expected to be the hottest point in the repository.

5.3 MODELLING RESULTS FROM THE NEAR-FIELD MODEL

Figure 22 shows the temperatures in the rock along the vertical surface near the placement room after 47 years. The temperature in the tunnel backfill material ranges between 83°C and 93°C.

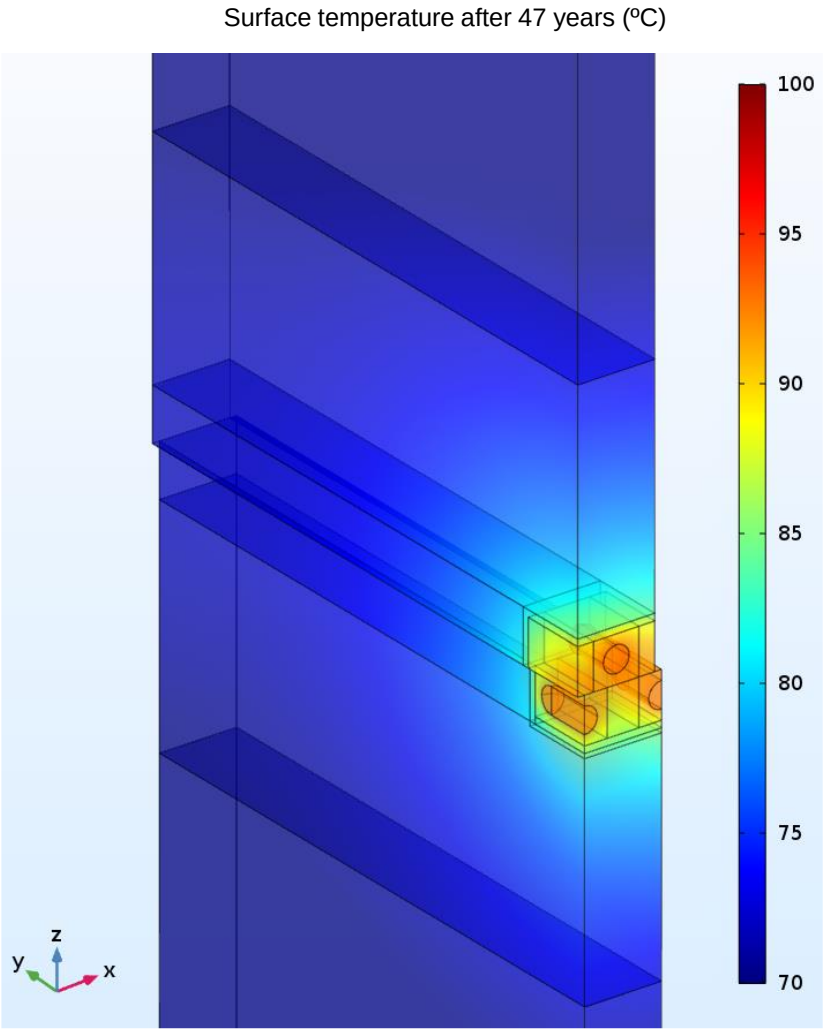

Figure 22: Temperatures in the Rock along the Vertical Surfaces near the Tunnel at Time of 47 Years after Placement

Figure 23 shows the temperatures along the horizontal cross-sections through the axis of the used fuel container after 47 years. The maximum container temperature of 93°C is reached at this time.

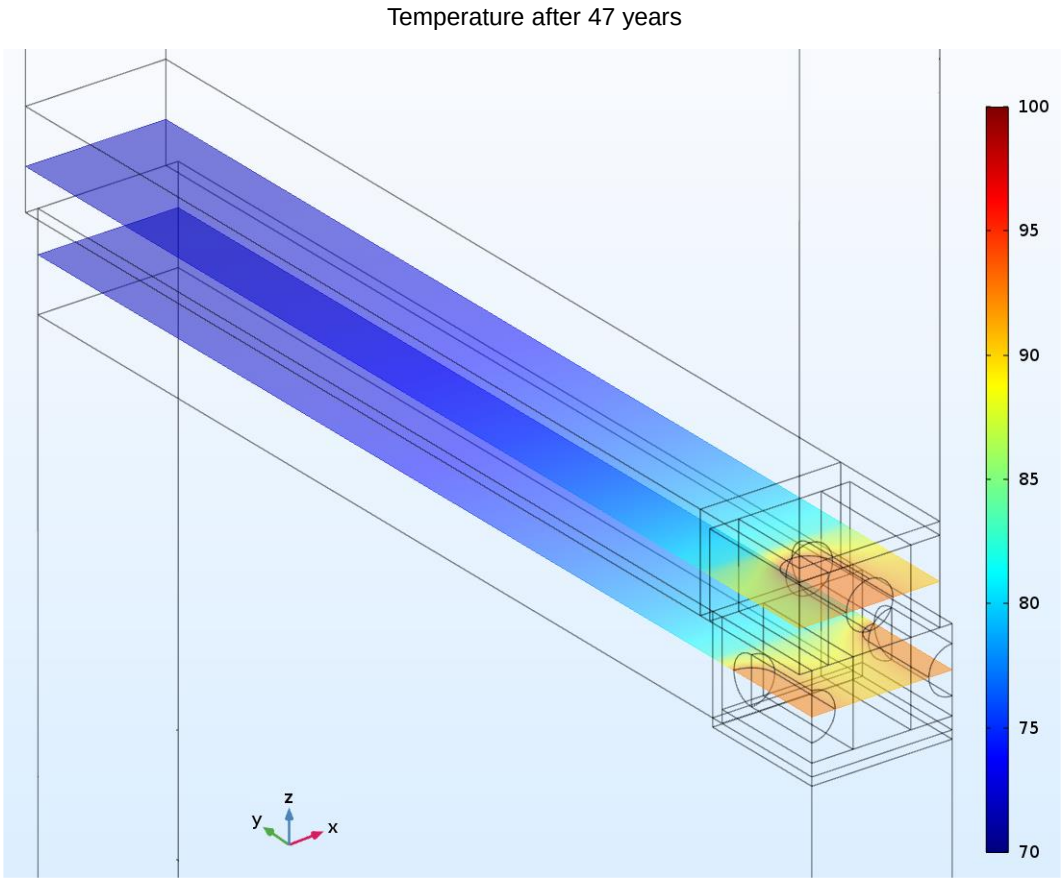

Figure 23: Temperatures in the Rock along Horizontal Cross-sections through the Container Axis at Time of 47 Years after Placement

Figure 24 shows the temperature comparison at the container surface and at the centre of the tunnel between the infinite Near-Field Model results and the near-field results. Dashed lines are from the infinite Near-Field Model and solid lines are from the near-field results. There is no second peak in the near-field temperature at the three locations.

The near-field container temperature now decreases from the first peak of 93°C at 47 years to 80.5°C at 600 years. The near-field temperature at tunnel centre (Point U_1, see Figure 17 for location) now decreases from the first peak of 92°C at 47 years to 80.3°C at 600 years. The near-field temperature at spacer block centre (Point U_2, see Figure 17 for location) decreases from the first peak of 90°C at 54 years to 79.8°C at 600 years. At 200,000 years, the near-field temperatures on the container surface, at the tunnel centre and at spacer block centre approach 17.8°C.

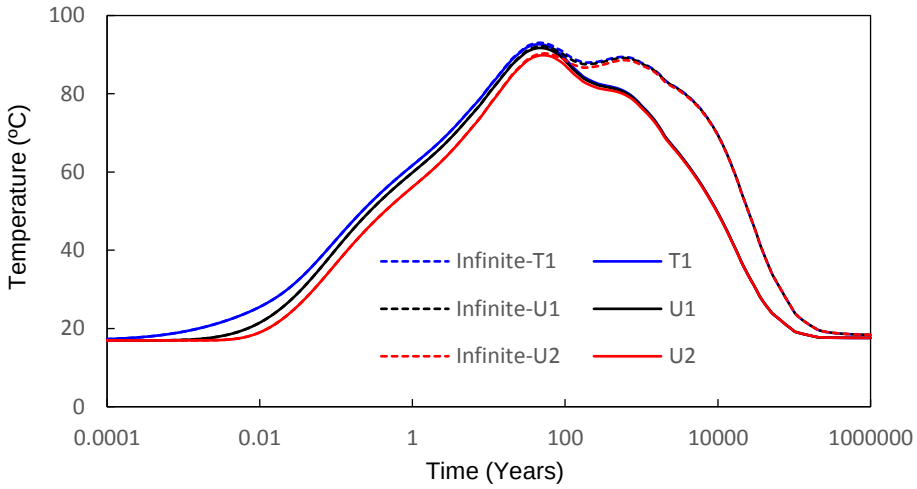

Figure 24: Comparison of the Temperature as a Function of Time at Points T_1 (container surface), Point U_1 (centre of tunnel) and Point U_2 (spacer block centre) between Infinite Near-Field Results and Near-Field Results

Figure 25 shows a comparison of temperature at Points V_0, V_1, V_2, V_3, and V_4, which are above the tunnel roof at 0 m, 2 m, 5 m, 10 m, and 30 m in the rock (see Figure 17 for locations), between the infinite near-field results and near-field results. The temperature of the rock roof above the top layer container from the infinite near-field modelling changes from the first peak of 85.3°C at 73 years to the second peak of 86.9°C at 647 years. The near-field temperature of the rock roof above the container now decreases from the first peak of 84.7°C at 68 years to 77.8°C at 650 years.

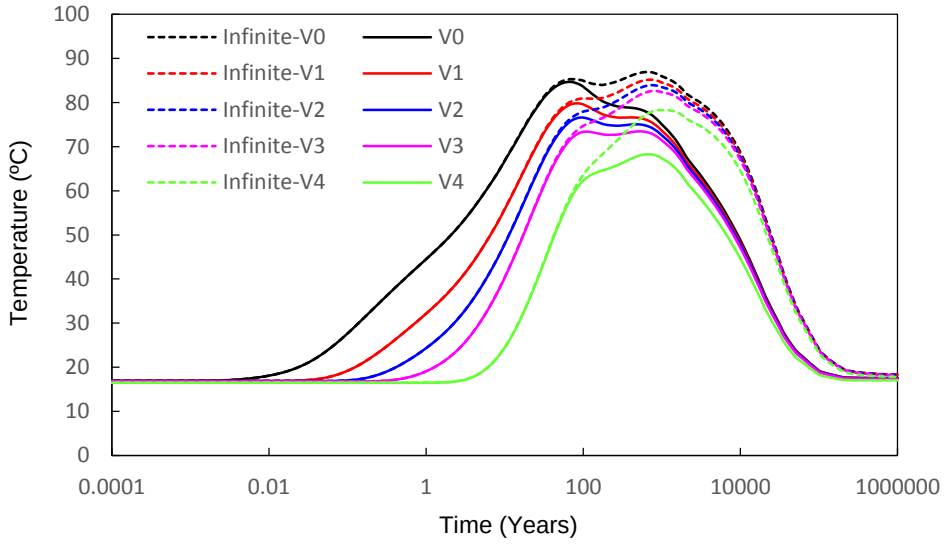

Figure 25: Comparison of the Temperature as a Function of Time at Points V_0, V_1, V_2, V_3 and V_4 between Infinite Near-Field Results and Near-Field Results

Figure 26 shows a comparison of temperature at Points X_1, X_2, X_3, and X_4 (see Figure 17 for locations), which are along the horizontal line facing the bottom container end at 0 m, 2 m, 5 m, 12.5 m in the rock, between the infinite near-field results and near-field results. The temperature of the rock wall facing the container end from the infinite near-field modelling changes from the first peak of 84.2°C at 87 years to the second peak of 86.5°C 700 years. The near-field temperature now decreases from the first peak of 83.5°C at 70 years to 77.1°C at 700 years.

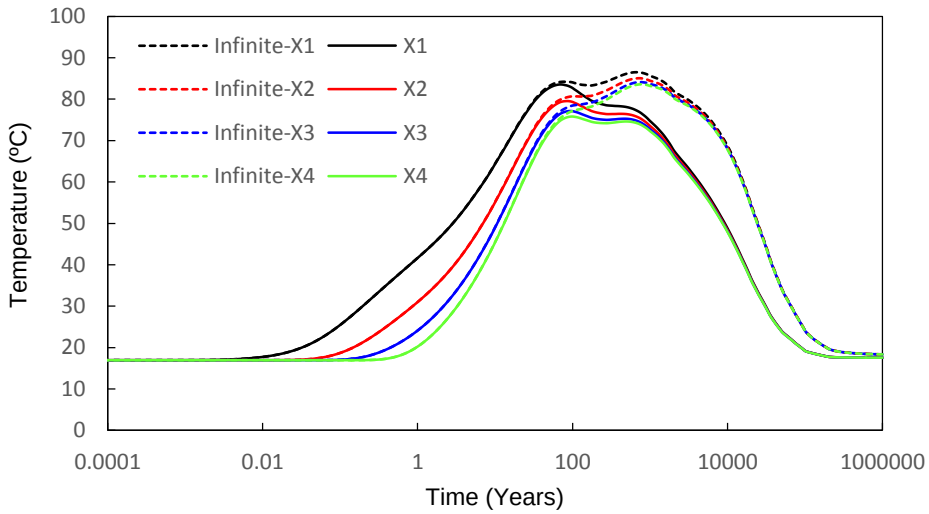

Figure 26: Comparison of the Temperature as a Function of Time at Points X_1, X_1, X_2 and X_3 between Infinite Near-Field Results and Near-Field Results

Figure 27 compares the temperature along a vertical line through top container centre in the Infinite Near-Field Model at 10,000 years, 25,000 years and 50,000 years to the near-field results and its initial temperature. Prior to 10,000 years, there is no influence of heat source or adiabatic boundary condition below a depth of 4000 m. At longer time, (i.e., after 50,000 years), the heat source from the repository does not influence the temperature below 4500 m, (due to its very low value at that time), but the influence of the adiabatic boundary condition extends to a depth of about 8000 m.

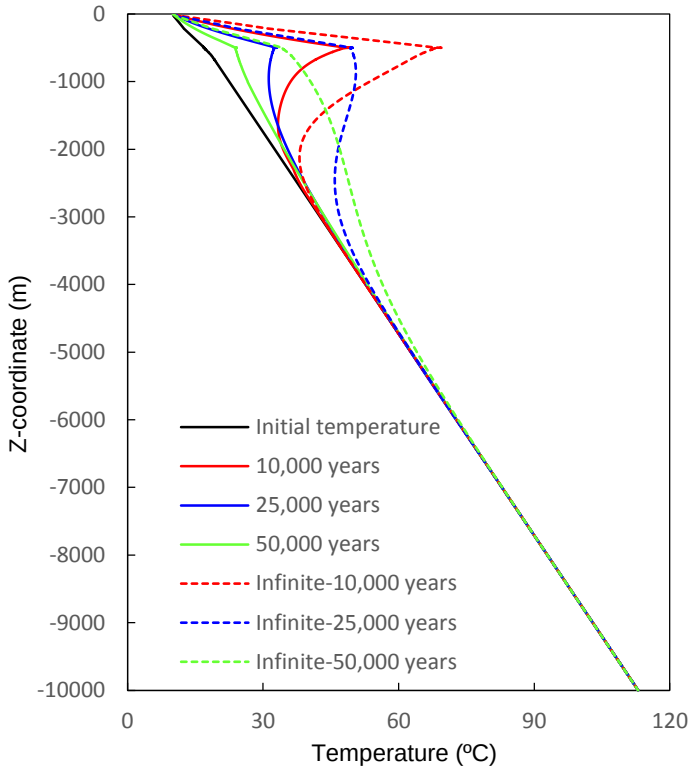

Figure 27: Comparison of the Infinite Near-Field and Near-Field Temperatures along Vertical Line through the Top Container Centre in the Near-Field Model

Figure 28 shows the container surface temperature difference caused by the adiabatic boundary conditions used in the near-field model at different locations in a panel near the repository centre (see Figure 5 for locations). At different locations, the adiabatic boundary condition induced temperature differences on the container surface are different.

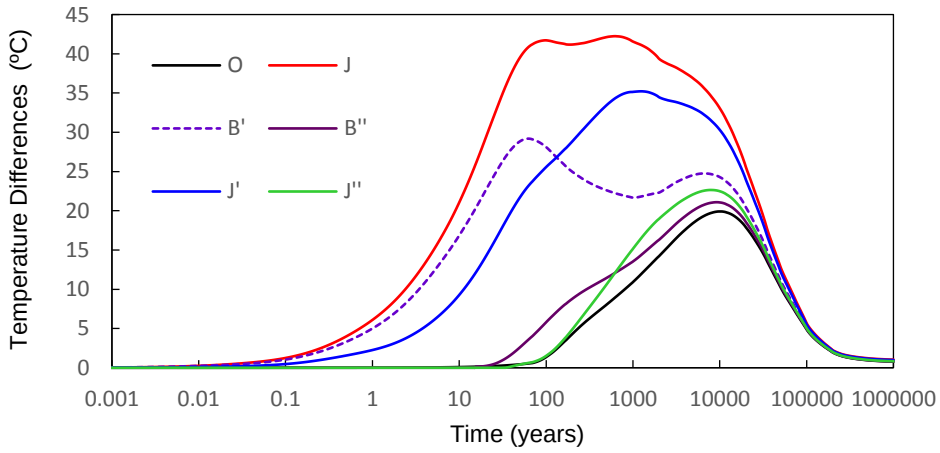

Figure 28: Temperature Differences at Different Points in the Panel near the Repository Centre

Figure 29 shows the container surface temperatures with time at different locations in a panel near the repository centre. The container surface temperature at different locations are different. For example, at Point O, the maximum container surface temperature is 93°C occurring at 44 years, at Point J″, the maximum container surface temperature is 92.8°C occurring at 43 years, at Point B″, the maximum container surface temperature is 91°C occurring at 36 years and at Point J, the maximum container surface temperature is 60°C occurring at 10 years.

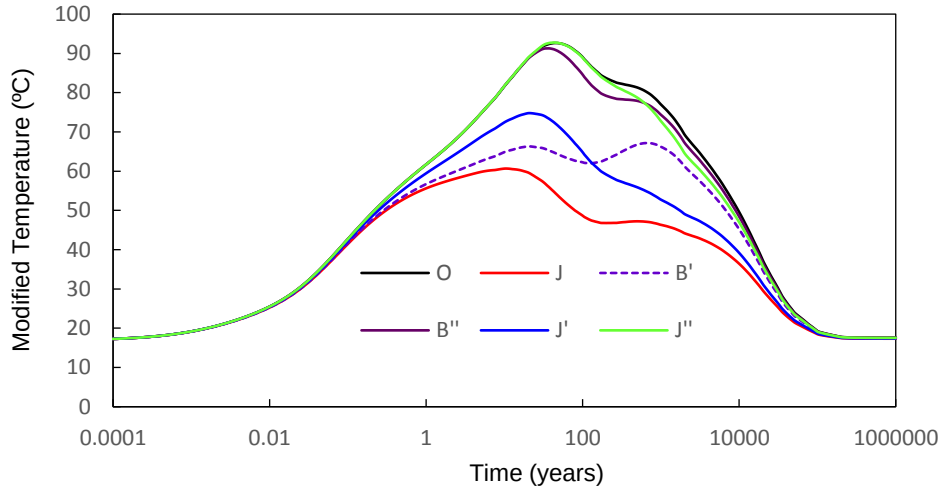

Figure 29: Temperatures at Different Locations in the Panel near the Repository Centre

Figure 30 shows the peak container temperatures at different locations in the repository and its time and the peak temperatures at the boundary of the Far-Field Model. The container temperature reaches a peak value of 93°C occurring after 43 years at all panel centres. The peak temperature is 60°C occurring after 10 years at all panel corners. The temperature at the middle of the longer side boundary of the centre panel (Point B′) has two peaks. One is 66°C occurring after 20 years and the second is 67°C occurring after 677 years. The maximum increase in temperature at the boundary of the model is only 0.8°C occurring after 29,000 years and this indicates that the Far-Field Model is of sufficient size for the thermal modelling.

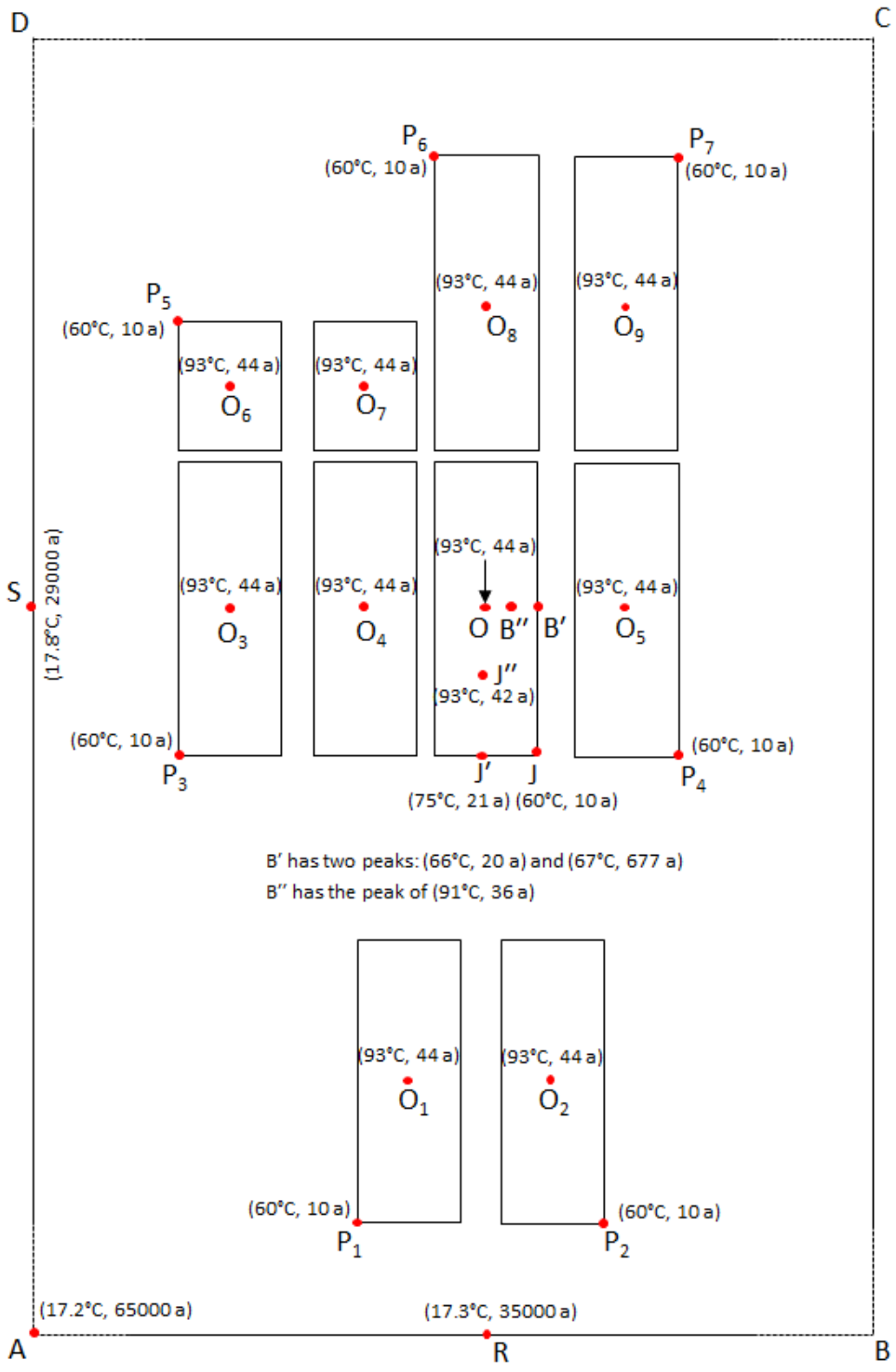

Figure 30: Peak Container Surface Temperature at Different Location in the Repository and its Time and Peak Rock Temperatures at Different Points along the Far-Field Model Boundary

In summary, the container surface temperature reaches its first peak of 93°C after 43 years and then decreases to 80.5°C after 600 years. The temperature at the placement room centre reaches its first peak of 92°C after 47 years and then decreases to 80.3°C after 600 years. The spacer block centre temperature decreases from its peak value of 90°C after 54 years to 80°C after 600 years.

The rock temperature at the roof of the tunnel above the container reaches its first peak of 84.7°C after 68 years and decreases to 77.8°C after 650 years.

The rock temperature at the middle wall of the tunnel reaches its first peak of 83.5°C after 70 years and its second peak of 77.1°C after 700 years.

After 100,000 years, the heat source from the repository only influences rock temperature above a depth of 4500 m (influence > 0.5ºC), while the influence of the adiabatic boundary condition used in the Near-Field Model extends to a depth of less than 8000 m.

The peak value of the temperature at the container surface is 93°C at all the panel centres. The peak value of the temperature at the container surface is 60°C at the panel corners.

6. INFLUENCE OF OTHER FACTORS ON THE THERMAL RESULTS

To better understand other factors which may affect container temperatures, this section studies the influences of buffer thermal conductivity, mesh size used in the COMSOL models, and the existence of the tunnels on the container surface temperature.

6.1 BUFFER THERMAL CONDUCTIVITY EFFECT

Based on Baumgartner (2006), the thermal conductivities of the highly compacted bentonite (HCB) used for the buffer box or spacer blocks and gap fill material (GFM) are functions of their saturation as shown in Figure 31. For the gap fill material, the minimum value of the thermal conductivity is 0.37 W/(m·K) occurring at a dried state and this value is used in the Near-Field Model as shown in Table 3. Therefore, the results from the near-field modelling are conservative regarding the gap fill material thermal conductivity.

For the HCB, a value of 1.0 W/(m·K) is used in the Near-Field Model; this value is the thermal conductivity of the HCB with its initial saturation. Due to heating, the thermal conductivity of the HCB near the container decreases with the decrease of its saturation in the first several years and then increases as saturation increases over time (Guo 2011). For the portion of the HCB far from the container, its thermal conductivity will increase due to its saturation increase. For the spacer blocks, these are sufficiently far from the container that their saturation is expected to only increase, and therefore their thermal conductivities will also only increase. The value of 1.0 W/(m·K) adopted for entire HCB system is therefore adopted as a conservative average value.

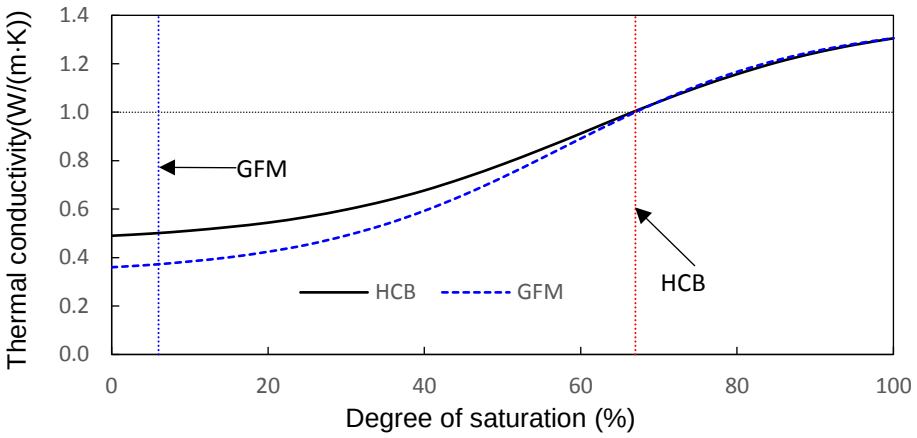

Figure 31: Relationship between the Thermal Conductivity and its Saturation for the Highly Compacted Bentonite (HCB) and Gap Fill Material (GFM)

In addition, two more conservative cases were run to study the influence of the thermal conductivity of the engineered sealing material on the thermal response in the repository. Case 1 represents the surrounding rock having a very low hydraulic permeability (e.g., sedimentary rock). Case 2 represents no inflow boundary condition for the engineered sealing materials (as bounding calculation).

For Case 1, the average of thermal conductivity of the buffer box decreases from its initial value of 1.0 W/(m·K) (equivalent to the saturation of 67%) to 0.72 W/(m·K) after 10 years (equivalent to the saturation of 45%) and then gradually increases to 1.3 W/(m·K) (equivalent to full saturation) after 4000 years, while the thermal conductivity of the gap fill material increases from its initial value to 1.3 W/(m·K) after 4000 years (Figure 32).

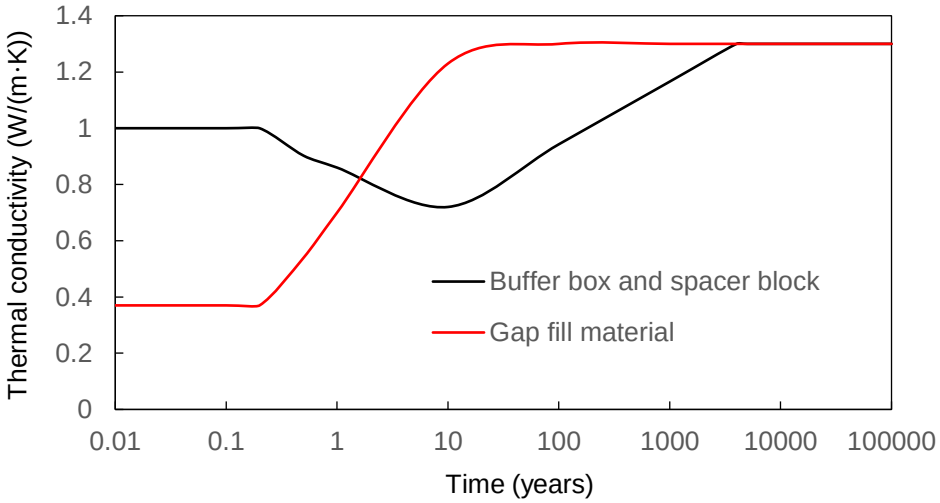

Figure 32: Thermal Conductivity of Buffer Boxes, Spacer Blocks and Gap Fill Material in Case 1

For Case 2, the average thermal conductivity of the buffer boxes and spacer blocks decreases from its initial value before 0.2 years to its lowest value of 0.5 W/(m·K) ("dry-out state") after 10 years. The moisture from the buffer boxes and spacer blocks migrates to the gap fill material and makes it be fully saturated after 10 years. The thermal conductivity used for the engineered sealing materials in Case 2 is shown in Figure 33.

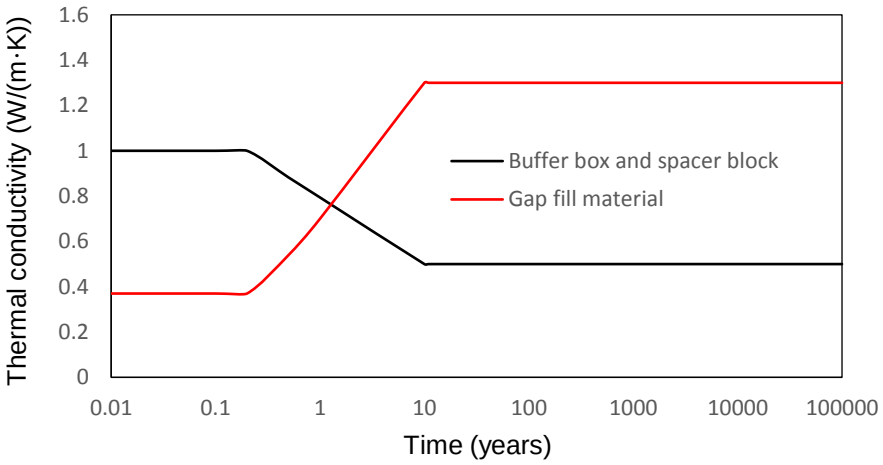

Figure 33: Thermal Conductivity of Buffer Boxes, Spacer Blocks and Gap Fill Material in Case 2

Figure 33 compared the top container surface temperatures from infinite near-field models for Case 1 and Case 2 with the case having the initial thermal conductivity for engineered sealing materials. Compared with Case 1 which is a more practical conservative case, the results in Section 5 (with initial thermal conductivity for engineered sealing materials) are more conservative. Although the value of the thermal conductivity for the engineered materials in Case 2 is not practical, it provides bounding value of 97°C of the container surface temperature.

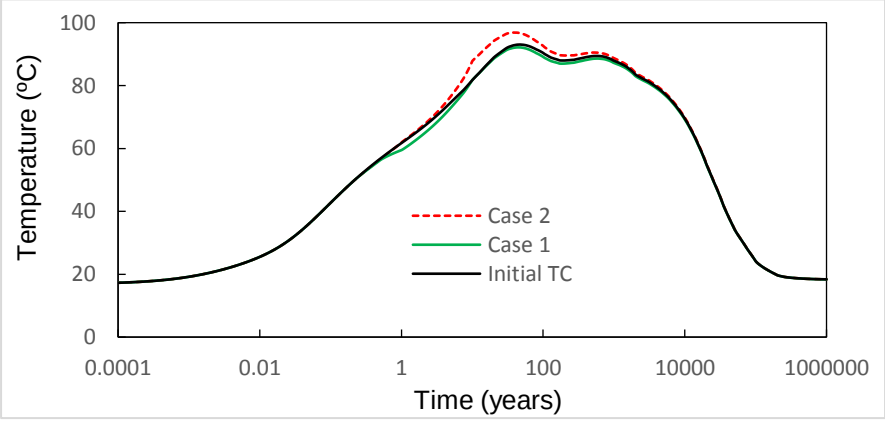

Figure 34: Influence of the Thermal Conductivity of the Clay-based Sealing Materials on Top Layer Container Surface Temperature

6.2 MESH SIZE EFFECT

In finite element analysis, it is known that mesh size can influence the modelling results. Figure 33 shows four meshes used in the near-field modelling. Mesh 1 is the coarsest mesh which has 6595 elements. The second coarse mesh has 22,847 elements. Mesh 3 and Mesh 4 have 70271 and 119642 elements, respectively. Mesh 3 is used in the near-field modelling (see Section 5.1.1)

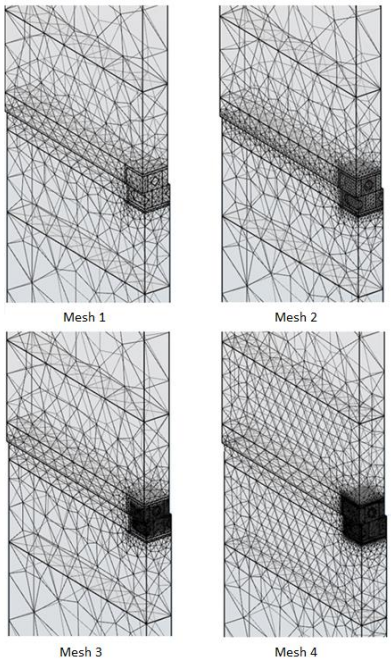

Figure 35: Four Meshes used in the Near-Field Models

Figure 34 shows the top container surface temperature as a function of time from the Infinite Near-Field Model using four different meshes. There is no difference in the modelled container surface temperature when using Mesh 2, Mesh 3 and Mesh 4. The results from the model using Mesh 1 are slightly higher than the other three meshes.

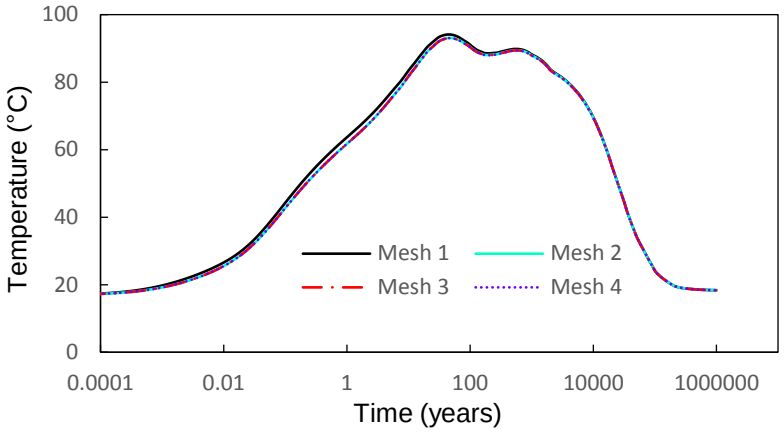

Figure 36: Top Container Surface Temperature as the Function of Time in the Infinite Near-Field Model using Four Meshes

Figure 35 shows the peak top container surface temperature as a function of element number. Once the element number is bigger than 30,000 in the Near-Field Model, the mesh influence is negligible. The Near-Field Model has 70721 elements and therefore, its results are deemed independent of mesh size.

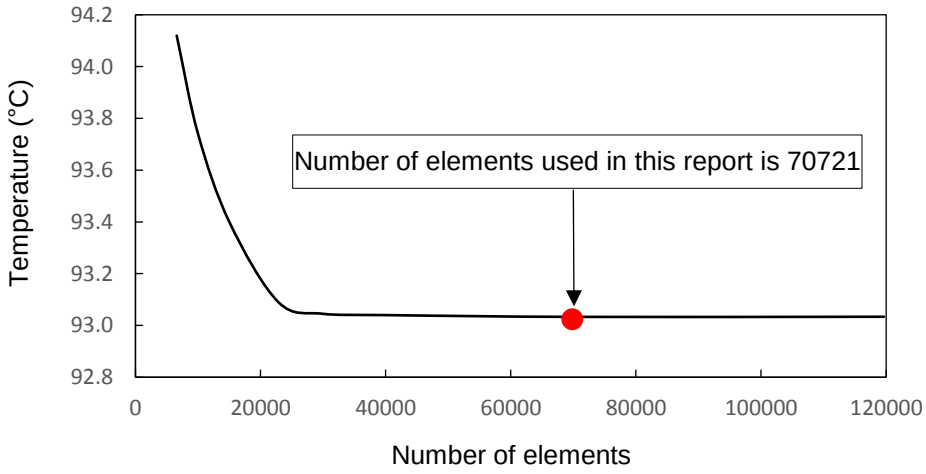

Figure 37: Peak Top Container Surface Temperature as a Function of Element Number

6.3 ACCESS TUNNEL EFFECT

In the modelling described in Section 4, the access tunnels are not represented. Due to the ventilation in the access tunnels, the repository temperature may be influenced.

Figure 36 shows the geometry of the COMSOL model which is used to analyze the influence of access tunnel ventilation. In the model, the main access tunnels are incorporated. In this model it is assumed that the tunnel temperature is 28°C for 30 years and again (in a separate simulation), for 100 years. (The assumed 28°C tunnel temperature is conservative, intended to represent a lower-ventilation-rate scenario.)

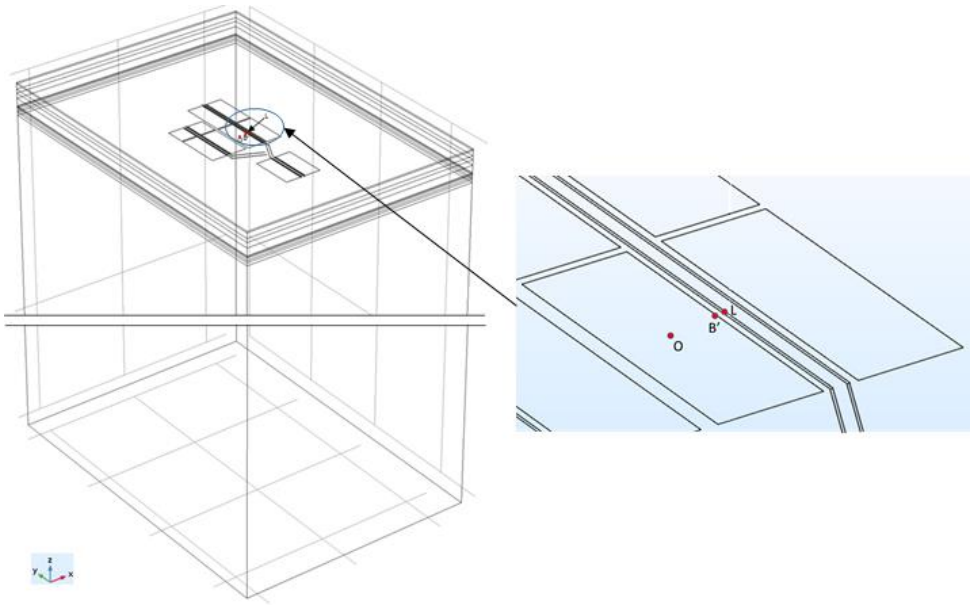

Figure 38: Far-Field Model Geometry with Placement Accesses

Figure 37 and Figure 38 show the comparison of the temperature at Point O with and without tunnels for 30 years and for 100 years, respectively. These comparisons indicate that the tunnel does not influence the panel centre temperature.

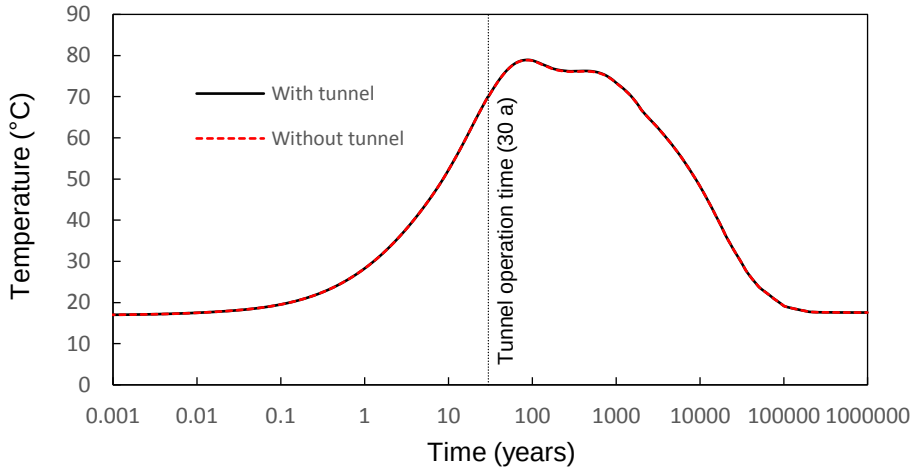

Figure 39: Influence of Tunnel Operation for 30 Years on the Temperature at Point O

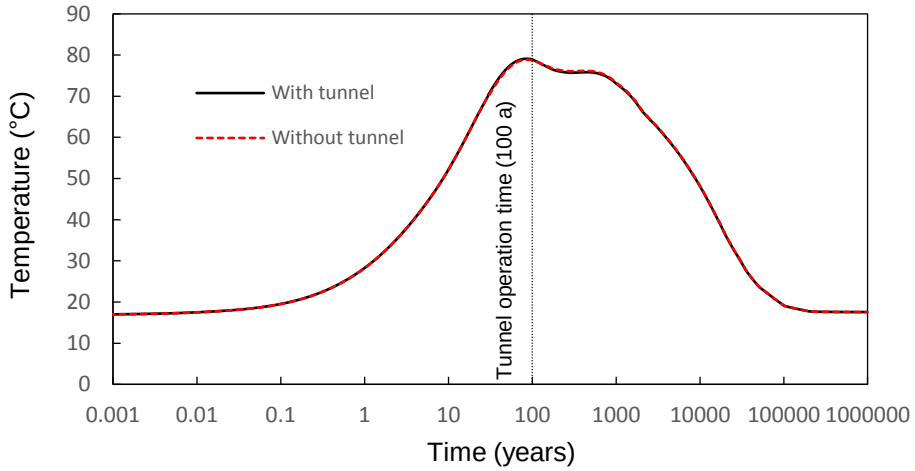

Figure 40: Influence of Tunnel Operation for 100 Years on the Temperature at Point O

Figure 39 and Figure 40 compare the temperature at Point B′ with and without the tunnels at 30 years and 100 years, respectively. If the tunnels are open for 30 years, the temperature at Point B′ increases due to the tunnel temperature being higher than the ambient temperature. The temperature increases less than 2.6°C. Once the tunnels are sealed, the temperature at Point B′ then gradually merges to the temperature for the case without the tunnel. If the tunnels are instead open for 100 years, the tunnel ventilation temperature is higher than the ambient temperature for the first 30 years and then lower than the ambient temperature thereafter. Therefore, the temperature at Point B' increases for the first 30 years and then decreases. The temperature decrease at Point B' can be 5.8°C. After 100 years, the temperature at Point B' gradually merges to the temperature for the case without tunnels represented.

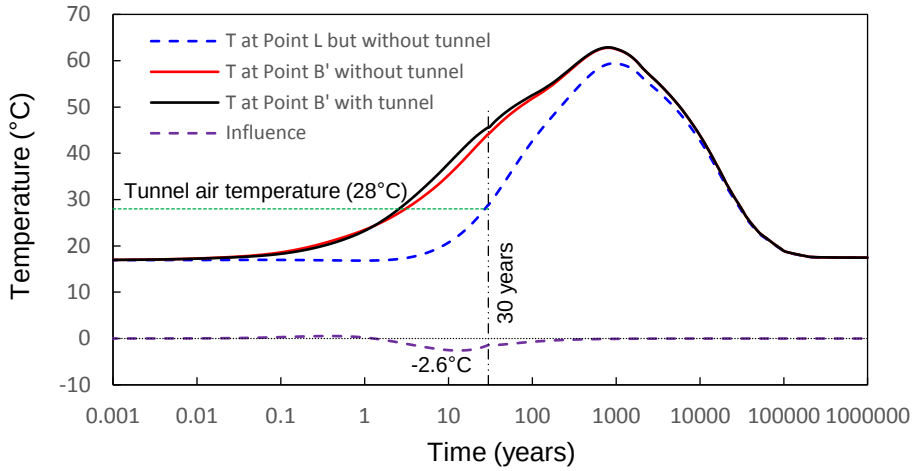

Figure 41: Influence of Tunnel Operation for 30 Years on the Temperature at Point B´

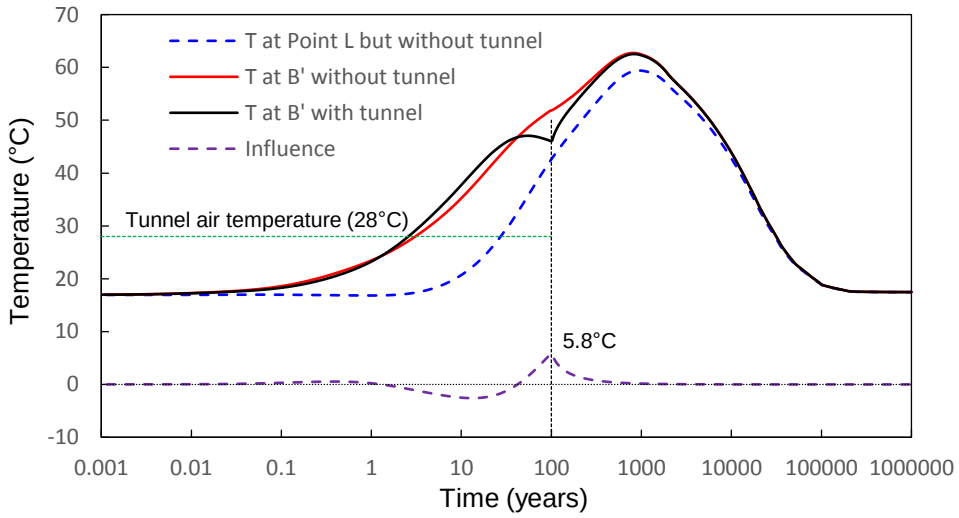

Figure 42: Influence of Tunnel Operation for 100 Years on the Temperature at Point B´

In summary, these sensitivity studies show that if low-moisture thermal conductivity is used for the buffer boxes and spacer blocks, the container temperature will not exceed 97°C. Furthermore, the mesh size used in this modelling exercise is fine enough to have no influence on the results. And finally, although representing the access tunnels can slightly change repository temperatures near the access tunnel locations, there is no influence on the temperature at the centre of a panel.

7. SUMMARY AND CONCLUSIONS

A series of three-dimensional finite-element thermal-transient analyses has been performed to gain a better understanding of the thermal response in the sealing materials and in the rock for the near-field and far-field areas of a conceptual repository in sedimentary rock.

The temperatures computed from the infinite Near-Field Model have been modified to correct for the influence of the adiabatic boundary condition. These near-field results can be used as input to near-field coupled thermal-mechanical modelling simulations.

The modelling results show:

- The container surface temperature reaches its peak of 93°C after 43 years and then decreases to 80.5°C after 600 years. After 200,000 years, the container surface temperature approaches 17.8°C (the ambient temperature is 17°C).
- The container surface temperature at panel corners reaches its peak of 60°C after 10 years.
- The placement room centre temperature reaches its peak of 92°C after 47 years and then decreases to 80.3°C after 600 years.
- The temperature at the placement room roof above the container reaches its peak of 84.7°C after 68 years and decreases to 77.8°C after 650 years.
- The temperature at the placement room wall facing the lower layer container end reaches its first peak of 83.5°C after 70 years and decrease to 77.1°C after 700 years.
- Assuming no influence means that the temperature increase is less than 0.5°C. Therefore, the heat load in the sedimentary repository thermally only influences the rock vertically to a maximum depth of 4.5 km from the repository centre after 100,000 years and the Far-Field Model shows that the used fuel heat load thermally influences the rock horizontally for a maximum distance of less than 2 km from the panel centre. The depth of the influence caused by adiabatic boundary condition reaches 8 km below the ground surface.

The presence of an access tunnel remaining open for 100 years has a small effect on repository temperatures at locations close to the tunnel. There is no effect on the maximum temperatures quoted above.

REFERENCES

Acres Consulting Services Limited in conjunction with RE/SPEC Ltd. 1985. A feasibility study of the multilevel vault concept. Atomic Energy of Canada Limited Technical Report, TR-297.

Acres Consulting Services Ltd. 1993. A preliminary study of long-hole emplacement alternatives. Atomic Energy of Canada Limited Technical Report, TR-346.

Baumgartner, P. 2006. Generic thermal-hydraulic-mechanical (THM) data for sealing materials, Volume 1: soil-water relationship. Ontario Power Generation, Nuclear Waste Management Division 06819-REP-01300-10122-R00.

Baumgartner, P., T.V. Tran and R. Burgher. 1994. Sensitivity analyses for the thermal response of a nuclear fuel waste disposal vault. Atomic Energy of Canada Limited Technical Report, TR-621, COG-94-258.

Berchenko, I., E. Detournay and N. Chandler. 1997. Propagation of natural hydraulic fractures. International Journal of Rock Mechanics and Mining Sciences 34(3/4) Paper no. 63.

COMSOL. 2017. Heat Transfer Module User's Guide. Version: COMSOL 5.3.

Dixon, D.A., N.A. Chandler, J. Graham and M.N. Gray. 2002. Two large-scale sealing tests conducted at Atomic Energy of Canada Limited's Underground Research Laboratory: the Buffer/Container Experiment and the Isothermal Test. Can. Geotech. J. 39, 503-518.

Golder Associates Ltd. 2013. OPG's deep geological repository for low and intermediate level waste factual report – Borehole DGR-7 and DGR-8, Geotechnical Logging. OPG 1011170042-REP-G2040-0004-01.

Gobien, M., F. Garisto, E. Kremer and M. Medri. 2017. Seventh Case Study: reference data and codes. Nuclear Waste Management Organization NWMO-TR-2017-15. (available at www.nwmo.ca).

Guo, R. 2007. Numerical modelling of a deep geological repository using the in-floor borehole placement method. Nuclear Waste Management Organization NWMO TR-2007-14. (available at www.nwmo.ca).

Guo, R. 2008. Sensitivity analyses to investigate the influence of the container spacing and tunnel spacing on the thermal response in a deep geological repository. Nuclear Waste Management Organization NWMO TR-2008-24. (available at www.nwmo.ca).

Guo, R. 2011. Thermohydromechanical modelling of the Buffer/Container Experiment. Engineering Geology 122, 303-315.

Guo, R. 2016. Thermal response of the Mark II conceptual deep geological repository in crystalline rock. Nuclear Waste Management Organization NWMO-TR-2016-03. (available at www.nwmo.ca).

Guo, R. 2017. Thermal response of a Canadian conceptual deep geological repository in crystalline rock and a method to correct the influence of the near-field adiabatic boundary condition. Engineering Geology, 218(2017) 50-62.

Holman, J.P. 1976. Heat Transfer, 4th edition. McGraw-Hill Book Company.

Hökmark, H., M. Lönnqvist, and B. Fälth. 2010. THM-issues in repository rock. Thermal, mechanical, thermos-mechanical and hydromechanical evolution of the rock at the

Forsmark and Laxemar sites. Swedish Nuclear Fuel and Waste Management Co, SKB TR-10-23.

Incropera, F.P. and D. P. DeWitt. 2002. Introduction to Heat Transfer, 5th ed., Wiley, New York.

Intera. 2011. Descriptive geosphere site model. Intera Engineering Ltd. Nuclear Waste Management Organization NWMO DGR-TR-2011-24 R0000.

King, F. 2013. Consequences of the general corrosion of carbon steel used fuel containers for gas generation in a DGR. Nuclear Waste Management Organization NWMO TR-2013-16. (Available at www.nwmo.ca).

Mathers, W.G. 1985. HOTROK, a program for calculating the transient temperature field from an underground nuclear waste disposal vault. Atomic Energy of Canada Limited Technical Report, TR-366.

NWMO. 2005. Choosing a way forward. The Future Management of Canada's Used Nuclear Fuel. Final study. Nuclear Waste Management Organization report submitted to the Minister, Natural Resource Canada. (Available at www.nwmo.ca).

Park, J.H., J.E. Kuh, S. Kwon, and C.H. Kang. 2000. Thermal analysis of high level radioactive waste repository using a large model. Journal of the Korean Nuclear Society, Vol. 32, No. 3, pp.244-253.

Radakovic-Guzina, Z., A. Riahi and B. Damjanac. 2015. Long-Term Stability Analysis of APM Conceptual Repository Design in Sedimentary and Crystalline Rock Settings. Nuclear Waste Management Organization NWMO-TR-2015-27. (Available at www.nwmo.ca).

Ranjith, P.G., D.R. Viete, B.J. Chen, and M.S.A. Perera. 2012. Transformation plasticity and the effect of temperature on the mechanical behaviour of Hawkesbury sandstone at atmospheric pressure. Engineering Geology 151, 120-127.

Read, R.S., J.B. Martino, E.J. Dzik, S. Oliver, S. Falls, and R.P. Young. 1997. Analysis and interpretation of AECL's Heated Failure Tests. Ontario Hydro Nuclear Waste Management Division Report No. 06819-REP-01200-0070-R00.

Tait, J.C., H. Roman and C.A. Morrison. 2000. Characteristics and radionuclide inventories of used fuel from OPG Nuclear Generating Stations. Volume 1 - Main report; and Volume 2 – Radionuclide inventory data. Ontario Power Generation Report 06819-REP-01200-10029-R00.

Tsui, K.K. and A. Tsai. 1985. Thermal analyses for different options of nuclear fuel waste placement. Atomic Energy of Canada Limited Report, AECL-7823.